Chapter

4

J Am Soc Nephrol, in press

Hematopoietic microRNA-126 protects against renal ischemia/reperfusion injury by promoting vascular integrity

Roel Bijkerk[1,2*], Coen van Solingen[1,2*], Hetty C. de Boer[1,2], Pieter van der Pol[1], Meriem Khairoun[1], Ruben G. de Bruin[1,2], Annemarie M. van Oeveren-Rietdijk[1,2], Ellen Lievers[1], Nicole Schlagwein[1], Danielle J. van Gijlswijk[1], Marko K. Roeten[1,2], Zeinab Neshati[3], Antoine A.F. de Vries[3], Mark Rodijk[4], Karin Pike-Overzet[4], Yascha W. van den Berg[2,5], Henri H. Versteeg[2,5], Marlies E.J. Reinders[1], Frank J.T. Staal[4], Cees van Kooten[1], Ton J. Rabelink[1,2] and Anton Jan van Zonneveld[1,2]

[1]Department of Nephrology and the [2]Einthoven Laboratory for Experimental Vascular Medicine, [3]Department of Cardiology, [4]Department of Immunohematology and Blood Transfusion, [5]Department of Thrombosis and Haemostasis, LUMC, Leiden, The Netherlands. *R.B. and C.V.S. contributed equally to this work.

Abstract

Ischemia/reperfusion injury (IRI) is a central phenomenon in kidney transplantation and acute kidney injury. Integrity of the renal peritubular capillary network is an important limiting factor in the recovery from IRI. MicroRNA-126 (miR-126) facilitates vascular regeneration by acting as an angiomir and by modulating mobilization of hematopoietic stem/progenitor cells. We hypothesized that overexpression of miR-126 in the hematopoietic compartment could protect the kidney against IRI via preservation of microvascular integrity. Here we demonstrate that hematopoietic overexpression of miR-126 increased neovascularization of subcutaneously implanted matrigel plugs in mice confirming its provasculogenic effects. Following renal IRI, mice overexpressing miR-126 display a marked decrease in urea levels, weight loss, fibrotic markers and injury markers such as KIM-1 and NGAL. This protective effect is associated with a higher density of the peritubular capillary network in the corticomedullary junction and increased numbers of bone marrow-derived endothelial cells. Hematopoietic overexpression of miR-126 increases the number of circulating $Lin^-/Sca\text{-}1^+/cKit^+$ hematopoietic stem and progenitor cells. In addition, miR-126 overexpression attenuates CXCR4 expression on $Lin^-/Sca\text{-}1^+/cKit^+$ cells in the bone marrow and increases renal expression of its ligand SDF-1, thus favoring mobilization of $Lin^-/Sca\text{-}1^+/cKit^+$ cells towards the kidney. Taken together, overexpression of miR-126 in the hematopoietic compartment is associated with SDF-1/CXCR4-dependent vasculogenic progenitor cell mobilization and promotes vascular integrity and support recovery of the kidney following IRI.

Introduction

Ischemia/reperfusion injury (IRI) is a central event in clinical conditions such as acute kidney injury and organ transplantation and is strongly associated with delayed graft function and long-term graft survival.[1-3] Emerging evidence indicates that the renal microvascular endothelium of the outer medullary peritubular network is the primary site of injury in the pathogenesis of ischemia-induced renal dysfunction.[4] Following ischemia, perfusion of the peritubular capillary network is rapidly impaired as a consequence of endothelial cell (EC) swelling,[5] impaired vasorelaxation[6] and increased leukocyte adhesion.[7] In addition, microvascular destabilization initiated by the loss of EC-EC-[8] and EC-pericyte interactions can lead to significant reductions in peritubular capillary density due to microvascular rarefaction.[8, 9] The resulting loss in renal perfusion can further exacerbate medullary ischemia and drive the development of interstitial fibrosis by stimulation of pro-fibrogenic factors such as transforming growth factor-β (TGF-β).[10] As a consequence, integrity of the peritubular capillary network is a key determinant for the preservation of renal function. Indeed, clinical biopsy studies have shown an association between loss of tubular structure and function on the one hand and capillary rarefaction on the other.[11, 12]

Due to their limited replicative capacity, renal ECs are thought to be insufficiently capable to completely repair the injured endothelium of the peritubular capillary plexus after IRI.[13, 14] Therefore, current therapeutic strategies to prevent microvascular loss have focused on the prevention of pericyte perturbation to reduce capillary rarefaction,[15-18] However, once rarefaction has occurred, these strategies may fail to induce sufficient revascularization required to reverse renal dysfunction.[19] In search of ways to augment neovascularization in the injured kidney many laboratories have investigated the biology and therapeutic use of circulating vascular progenitor cells originating from the bone marrow (BM) compartment.[20] These progenitor cells were shown to incorporate into the injured microvasculature in experimental models for glomerulonephritis,[21] ischemic nephropathy[22, 23] and interstitial fibrosis.[24] This phenomenon has been particularly observed when extensive or repetitive endothelial injury occurs, for example in kidney transplantation.[25] Microvascular incorporation of BM-derived progenitor cells has been linked to preservation of the vasculature as they may serve as an alternative cellular source to facilitate re-endothelialization.[26] In addition, the $CXCR4^+$ fraction of progenitor cells is mobilized to the ischemic kidney by local secretion of the chemokine stromal cell-derived factor-1 (SDF-1)[23,27]

and has been shown to exert renoprotective effects in a paracrine fashion. PI3K/AKT signaling in progenitor cells plays a critical role in mobilization of progenitors from the BM via the SDF-1/CXCR4 axis[28] and their subsequent differentiation towards vascular cells.[30] MicroRNA-126 (miR-126) is a key regulator of PI3K/AKT signaling by direct targeting of the negative regulator PI3K regulatory subunit 2 (PI3KR2/p85-β) and targets genes that play key roles in angiogenesis and inflammation.[29-31] In addition, miR-126 was shown to co-regulate the expansion and mobilization of hematopoietic stem/progenitor cells.[32, 33] We hypothesized that miR-126 overexpression in the hematopoietic compartment of mice can enhance the vasoprotective potential of these progenitors and this will translate to decreased renal injury.

Results

Generation of mice overexpressing miR-126 in the hematopoietic compartment

To investigate the pro-vasculogenic effect of miR-126, we generated mice overexpressing miR-126 in the hematopoietic compartment. To that end, mice were transplanted with lineage-negative enriched CD45.1^{+} BM cells transduced with a lentiviral vector (LV) driving the expression of miR-126 and dsRed under control of a constitutive human U6 and a phosphoglycerate kinase 1 (PGK1) promoter, respectively (Supplementary Figure 1). Eight weeks after transplantation, mice were sacrificed and blood and BM samples were obtained. Smears of peripheral blood (PB) and BM of transduced animals showed dsRed-positivity, confirming the successful transduction of the transplanted BM (Figure 1A). FACS analysis for the expression ratios between congenic markers CD45.1 (donor) and CD45.2 (acceptor) in PB and BM of the transplanted mice demonstrated high levels of chimerism (Figure 1B), as CD45.1 expression in the control group (LV-C) and miR-126 overexpression group (LV-126) was similar to CD45.1 expression in donor mice. Quantitative PCR (qPCR) confirmed a 5.1- (Figure 1C, $P<0.001$) and 6.0-fold (Figure 1D, $P<0.05$) higher expression level of miR-126 in BM and PB cells, respectively, in the LV-126 group compared to the LV-C group. Finally, confirming downstream effects of miR-126 over expression, we observed that mRNA levels of 7 out of 9 established miR-126 targets in total BM were reduced in the LV-126 group compared to LV-C controls (Supplementary Figure 2).

Hematopoietic overexpression of miR-126 increases neovascularization of subcutaneously implanted angiogenic matrigel plugs in mice

To assess the impact of hematopoietic overexpression of miR-126 on vasculogenesis, we performed *in vivo*, angiogenic matrigel plug assays. Therefore, 7 weeks after BM transplantation, matrigel plugs enriched with recombinant pro-angiogenic factors SDF-1 and vascular endothelial growth factor (VEGF), were subcutaneously implanted in the flanks of LV-126 and LV-C mice. After 7 days, the skin was opened to visualize the neovasculature of the implants by a sidestream dark field camera. Movies (Figure 2B) confirmed the ingrowth of functional neovasculature with active flow of red blood cells. To quantify the extent of neovascularization, microscopic images were taken from both sides of the angiogenic plugs. Figure 2A shows a panel of representative microphotographs, with arrowheads indicating the blood-filled microvascular structures that had formed in the matrigel plugs following

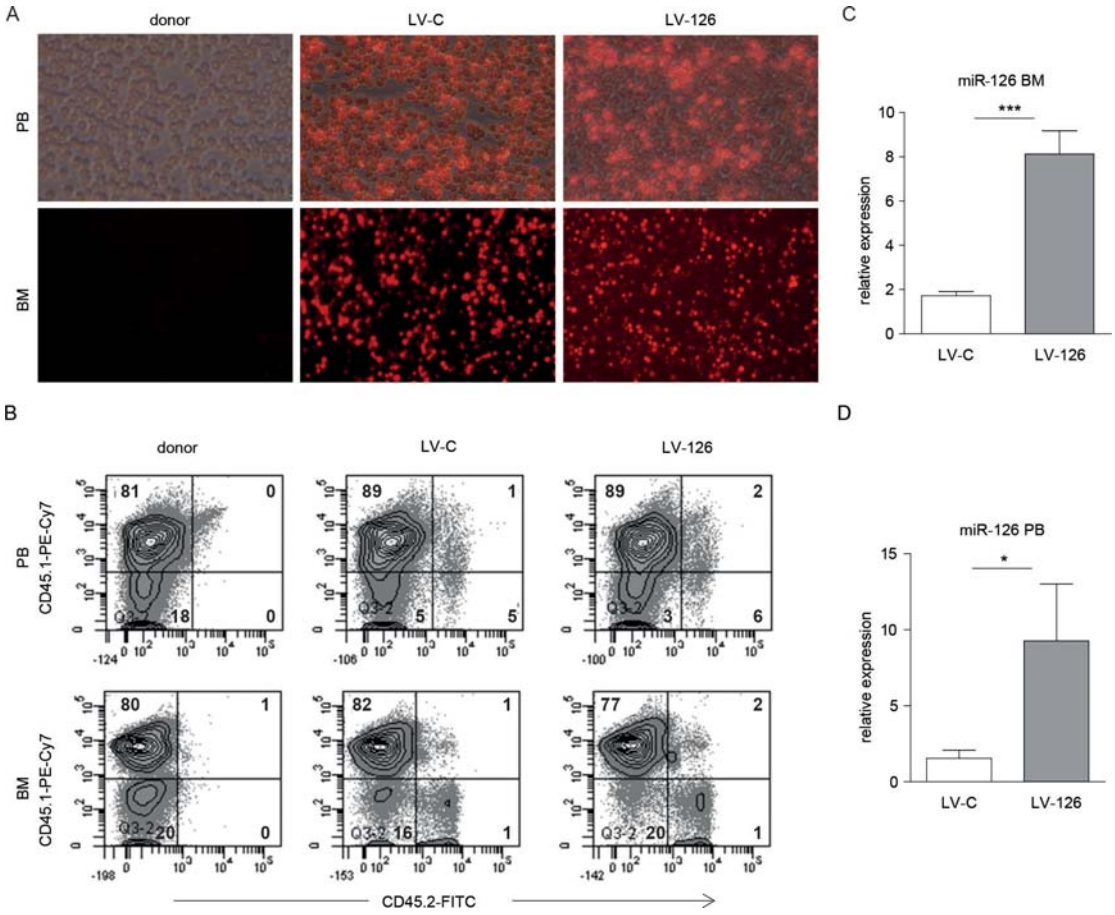

Figure 1. Overexpression of miR-126 and BM transplantation in vivo. (A) Microscopic images of peripheral blood (PB) and bone marrow (BM) smears show dsRed+ cells in animals transplanted with either LV-C or LC-126 when compared to cells of non-transplanted animals (donor). (B) Representative FACS plots demonstrate successful chimerism in PB and BM by CD45.1 (donor) and CD45.2 (acceptor) levels. Numbers represent percentage of cells in corresponding quadrant. qRT-PCR demonstrates significant upregulation of miR-126 levels in BM (C) and PB (D) of LV-126 mice when compared to LV-C mice.

implantation. Using these photographs we counted the number of vessels per matrigel implant and observed a nearly significant increase in the number of vessels in the LV-126 mice as compared to the LV-C animals (Figure 2C, n=10, P=0.053). Moreover, quantification of the total microvascular surface area revealed a significant increase (40%) in vascularization in the LV-126 mice (Figure 2D, P<0.02), which correlated directly with the levels of miR-126 expression in the BM of the mice (Figure 2E, P=0.05, $r^2 = 0.20$). Immunohistological analyses of the vascularized matrigel plugs (Figure 2F-G) demonstrated stabilized, maturing vessels and a profound infiltration of BM-derived, dsRed$^+$ cells that overlap with staining for murine EC antigen-32

(MECA32) or von Willebrand Factor (vWF)(Figure 2F and Supplementary Figure 3A). Around the newly formed blood vessels, cells positive for platelet derived growth factor receptor β (PDGFRβ) and neural/glial antigen 2 (NG2)(Figure 2G and Supplementary Figure 3B) were detected, which were also positive for dsRed, suggesting a BM origin.

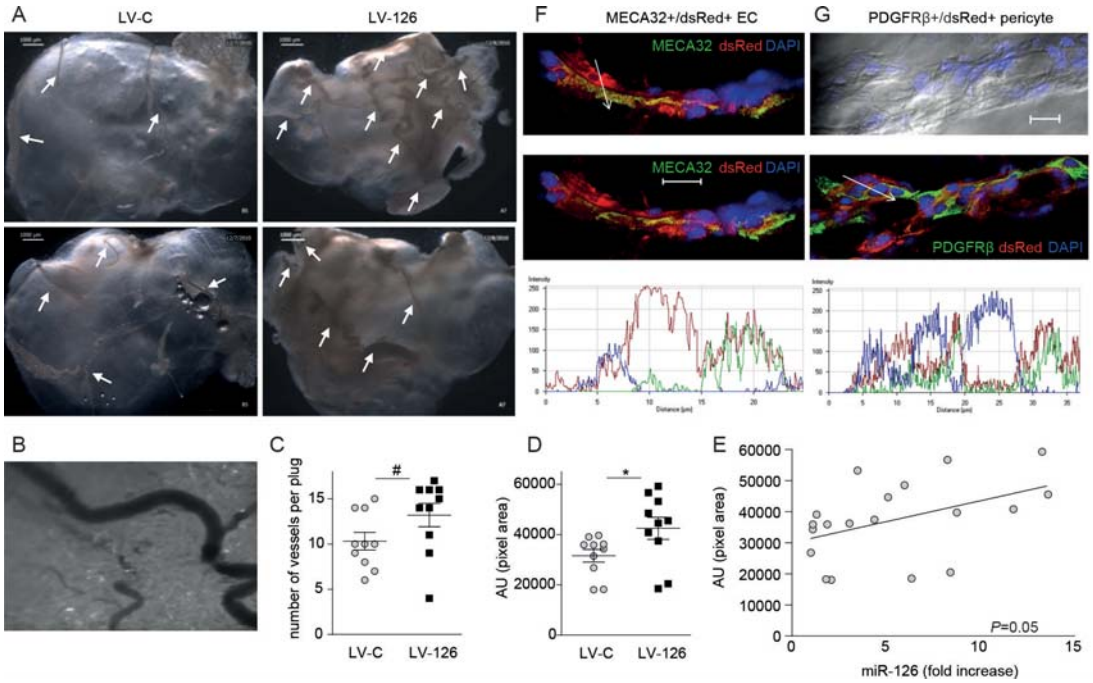

Figure 2. Overexpression of miR-126 in BM cells leads to increased neovascularization in subcutaneously implanted matrigel plugs. (A) Representative microscopic images of both sides of matrigel plugs seven days after implantation in LV-C mice (left micrographs) and LV-126 mice (right micrographs). Arrowheads point to neovasculature. (B) A movie still displaying the presence of red blood cells in the neovasculature of the matrigel plugs. (C) Quantification of the number of vessels per plug shows increased vascularization in animals transplanted with LV-126 BM with borderline significance (P=0.053). (D) Vessels were 'digitalized' and the total length (in pixel area) was quantified. LV-126 animals demonstrated a significantly higher vessel surface area as compared to LV-C animals. (E) Total surface area of plug-vessels correlates significantly with the expression levels of miR-126 in the BM (P=0.05). (F-G) Representative confocal images of a vessel and corresponding cross sectional profiles of fluorescent labels (colors correspond to images) stained for MECA32+/dsRed+ EC in 2 different planes (F) and stained for PDGFRβ+/dsRed+ pericytes (G). *P<0.01, #P<0.10.

Our data indicate that overexpression of miR-126 in the hematopoietic compartment stimulates neovasculogenesis of implanted matrigel plugs that possibly involves both BM-derived EC as well as BM-derived perivascular cells.

MiR-126 overexpression in the hematopoietic compartment protects against renal IRI

Given the observed pro-vasculogenic effects in mice overexpressing miR-126 in the hematopoietic compartment we hypothesized that these mice would be less susceptible to IRI due to an improved capacity to maintain renal microvascular integrity. To investigate this hypothesis, 8 weeks after BM transplantation, LV-126 and LV-C mice were subjected to bilateral renal ischemia and were sacrificed 3 days or 3 weeks after the procedure. Renal IRI resulted in extensive renal dysfunction in the LV-C mice as shown by increased blood levels of urea (Figure 3A). In contrast, mice overexpressing miR-126 were protected against renal dysfunction, with a moderate elevation in urea levels as compared to control mice. At 72 h after reperfusion this deterioration of renal function in the LV-C mice was accompanied by a significantly lower weight than the LV-126 mice (Figure 3B) and significantly lower mRNA levels of the tubular injury markers kidney injury molecule-1 (KIM-1) and neutrophil gelatinase-associated lipocalin (NGAL), pro-inflammatory markers interleukin-6 (IL-6) and chemokine (C-C motif) ligand 2 (CCL2), and upregulation of anti-inflammatory cytokine interleukin-10 (IL-10) (Figure 3C). In addition, analyses of post-IRI, H&E stained kidney sections revealed that mice in the LV-126 group displayed significantly less acute tubular necrosis (ATN) and tubular cast formation (rating 0-3) compared to the LV-C mice (Figure 3E). Direct immunohistochemical staining confirmed a markedly lower expression of tubular injury marker KIM-1 (2.6-fold) in the LV-126 group (Figure 3F, $P<0.001$). Tubular injury after reperfusion was accompanied by extensive infiltration of $CD45^+$ leukocytes (Figure 3G). However, overexpression of miR-126 did not reduce the total number of infiltrating leukocytes, neither did it affect the total number of $F4/80^+$ macrophages (Figure 3H). In contrast, we did find a decrease in the presence of $Gr1^+$ granulocyte count as a result of overexpression of miR-126 (Figure 3I). As miR-126 has been described to positively regulate mast cell proliferation and cytokine production,[34] we stained the sections with toluidine blue to determine the mast cell content of the kidneys, but could not observe any positive mast cell staining in the kidneys of either group (data not shown).

To determine whether the early protective effects observed in the LV-126 group also have beneficial effects on the longer-term fibrotic complications of IRI[35] we measured gene expression levels of fibrosis markers Collagen-1α1 (Col1α1), Collagen-3α1 (Col3α1) and TGF-β, and of the myofibroblast marker α-smooth muscle actin (α-SMA) in mice that were sacrificed 3 weeks after reperfusion. Indeed, we confirmed that expression of each of these

markers was significantly reduced in the kidneys from the LV-126 group compared to those of the LV-C mice (Figure 3D).

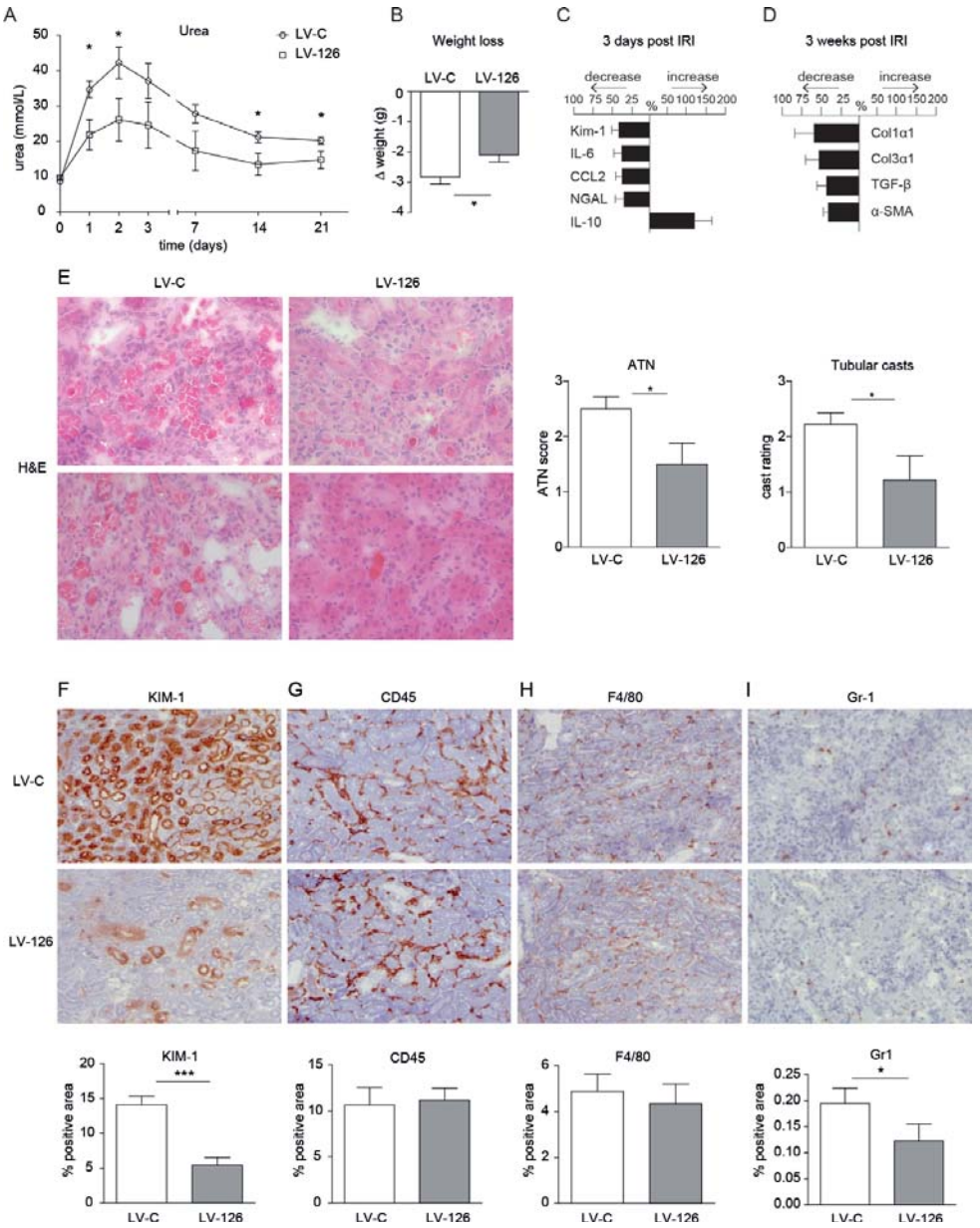

Figure 3. miR-126 protects against renal IRI. (A) miR-126 overexpression results in decreased blood urea levels after IRI. (B) miR-126 overexpression results in less weight loss 3 days after IRI. qRT-PCR analysis normalized on GAPDH mRNA levels of renal gene expression in LV-126 and LV-C mice of (C) KIM-1, NGAL, CCL2, IL-6 and IL-10 3 days after injury and (D) -SMA, col1a1, col3a1 and TGF-β 3 weeks after injury. Increase or decrease is relative to LV-C group. (E) Representative images of H&E staining on LV-C and LV-126 kidney sections. Graphs show quantification of ATN and cast score. (F-I) Representative images of staining for tubular damage (E, KIM-1), leukocytes (F, CD45), macrophages (G, F4/80) and neutrophils (H, Gr-1) 3 days after IRI. Graphs below images show quantification of staining results for all mice (n=10 per group).

Hematopoietic overexpression of miR-126 preserves capillary density after IRI and is associated with increased numbers of BM-derived peritubular capillary EC

To determine the impact of hematopoietic miR-126 overexpression on renal vascular integrity after IRI, we assessed the density of the peritubular capillary network by staining for MECA32 before and after IR. We focused on the corticomedullary junction since it is known that this region is disproportionally damaged by IRI.[4] As shown in Figure 4A and 4E we observed that the density of MECA32+ peritubular capillaries in the LV-C mice was markedly decreased three days post-IR, while microvascular density was virtually maintained in the LV-126 mice (Figure 4G). Since both the control- and miR-126 viral vectors carried the dsRed reporter gene, BM-derived cells could be identified based on their dsRed positivity. Notably, a 2.2-fold increase was observed in the number of $dsRed^+$ BM-derived cells in the kidneys of the LV-126 mice as compared to the LV-C group (Figure 4B and 4H). Importantly, this increase was IR-dependent, as the number of $dsRed^+$ cells in the LV-126 mice in the non-IR group was comparable to that of the LV-C mice (Figure 4F-H). Since no differences were observed in the numbers of infiltrated CD45 leukocytes or the macrophage content between the two experimental IRI groups, we sought to determine the cell type that could be responsible for the increase in $dsRed^+$ cells. Based on the interstitial localization of the $dsRed^+$ cells we could exclude that they were tubular epithelial cells. Double staining of kidneys for dsRed and the endothelial marker CD31 demonstrated that a major fraction of the BM-derived $dsRed^+$ cells were ECs (Figure 4C). Quantification of these BM-derived capillary EC ($CD31^+/dsRed^+$) showed a significant 2.0-fold increase (P=0.04) in the LV-126 group compared to the control group (Figure 4D).

Confocal imaging confirmed the presence of BM-derived ECs as we readily detected numerous $dsRed^+$ cells co-staining for MECA32 integrated into networks of $MECA32^+/dsRed^-$ ECs (Figure 4I-K). In concordance with the results of the matrigel plug assay, also in the kidney we observed co-localization of dsRed and PDGFRβ (Supplementary Figure 4). $DsRed^+CD31^+$ cells were also found in the endothelium of the larger vessels (Supplementary Figure 5A) and at a lower rate in the glomeruli of the LV-126 mice (Supplementary Figure 5B). We conclude that overexpression of miR-126 in the hematopoietic compartment aids to preserve the integrity of the renal microvasculature following IRI and associates with an increased incorporation of BM-derived cells into the vasculature.

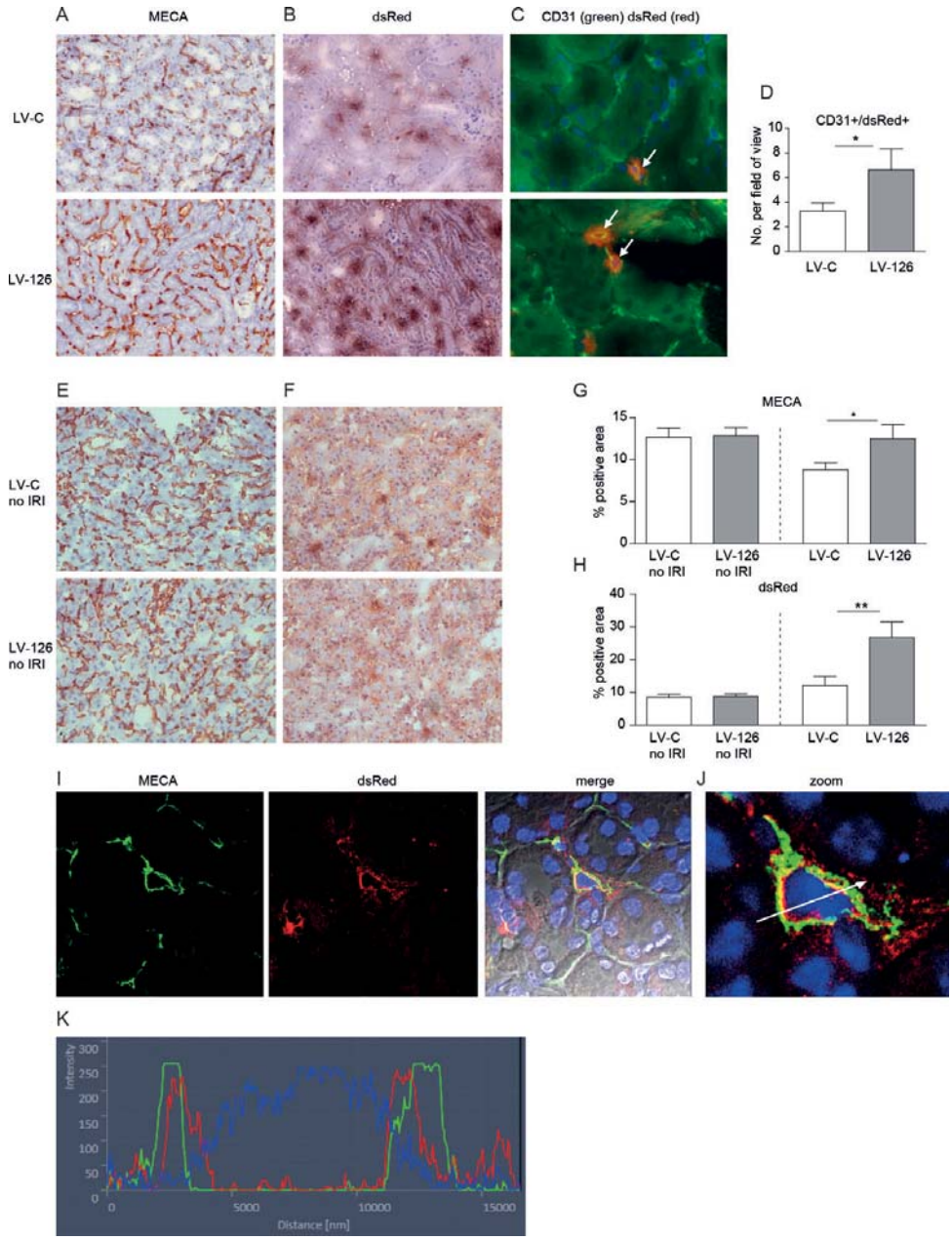

Figure 4. MiR-126 preserves capillary density by increasing incorporation of BM-derived EC. (A) Representative microscopic images and (G) quantification of MECA32 staining in corticomedullary junctions show higher capillary density in mice that overexpress miR-126 3 days after IRI. (B) Representative microscopic images and (H) quantification of dsRed staining in the kidney show increased dsRed signal in LV-126 mice. (C) Representative images showing CD31+/dsRed+ cells as indicated by arrows and (D) quantification shows higher numbers of BM- derived EC in the miR-126 group. (EF) Representative microscopic images and (GH) quantification of MECA32 and dsRed staining in corticomedullary junctions of non-ischemic kidney shows no differences as a result of miR-126 overexpression. (I) Confocal images confirm dsRed-positive ECs by MECA staining. (J) Zoomed image of dsRed+ EC and corresponding cross sectional profile of fluorescent labels (K, colors correspond to images) shows overlap of MECA32 and dsRed.

LV-126 mice display increased hematopoietic stem- and progenitor cell numbers in the circulation following IRI

After having shown the provasculogenic effects of BM miR-126 overexpression in the matrigel plug assay and in the kidney after IRI, we assessed the impact of miR-126 overexpression on the hematopoietic system itself. Therefore, a detailed comparison was performed of the composition of cells in the BM and in the circulation in LV-126 and LV-C mice (Supplementary Table 1 and 2). Little to no differences were observed in the number of white blood cells (WBCs), red blood cells (RBC), platelets (plt), hemoglobin (Hgb) or hematocrit (Hct) content between the two experimental groups in blood samples collected before and 4 and 8 weeks after BM transplantation. Also, no substantial differences were found in absolute numbers of T-cells, B-cells, NK-cells, plasmacytoid dendritic cells (pDCs), neutrophils or eosinophils. Since circulating myeloid cells are known to display pro-angiogenic properties[36] and we previously demonstrated that pro-angiogenic cells could be cultured from a BM-derived immature, $CD31^+/Ly6C^{hi}$ myeloid progenitor cell fraction[37], the monocytic cells were further subdivided into $Ly6C^{hi}$, $Ly6C^{med}$ and $Ly6C^{lo}$ fractions but again, no significant differences could be observed between the experimental groups. Next, we assessed the impact of overexpression of miR-126 on the number of $Lin^-/Sca\text{-}1^+/cKit^+$ (LSK) and $Lin^-/Sca\text{-}1^+/Flk^+$ (LSF) hematopoietic stem/progenitor cells in PB and BM, before (pre-IRI) and 3 days after kidney IRI. While the absolute numbers of circulating LSK (Figure 5A) or LSF cells (Figure 5B) before kidney IRI did not differ significantly between the experimental groups, three days after IRI, the LSK and LSF cells in PB were induced 2.5- and 1.5-fold respectively ($P<0.05$ for both). Concomitant with their elevation in the circulation, BM-levels of the LSK and LSF cells were decreased, supporting enhanced mobilization of these cells from BM to the periphery after overexpression of miR-126.

Correlation analysis (Table 1) revealed a strong positive correlation between the expression level of miR-126 in the BM and LSK cell number in PB. The number of LSK cells correlated positively with capillary density (MECA staining) in the kidney, while strong negative correlations were observed with renal injury markers (urea, KIM-1, NGAL) further supporting that miR-126 is the driver of the observed protective effects.

CXCR4/SDF-1 signaling is affected in LV-126 mice after IRI

Since the mobilization of LSK and LSF cells was markedly increased in the LV-126 mice we sought to determine whether overexpression of miR-126 in the hematopoietic compartment was also associated with a shift in the balance between BM and peripheral SDF-1/CXCR4 signaling. As CXCR4

expression retains hematopoietic stem and progenitor cells in the BM and its inhibition can be employed to mobilize these cells from the BM,[38] we measured CXCR4 expression on BM-LSK cells using flow cytometry. Indeed, CXCR4 expression was selectively reduced on BM-LSK cells in the LV-126 group, while Lin^+ cells showed an elevated expression of CXCR4

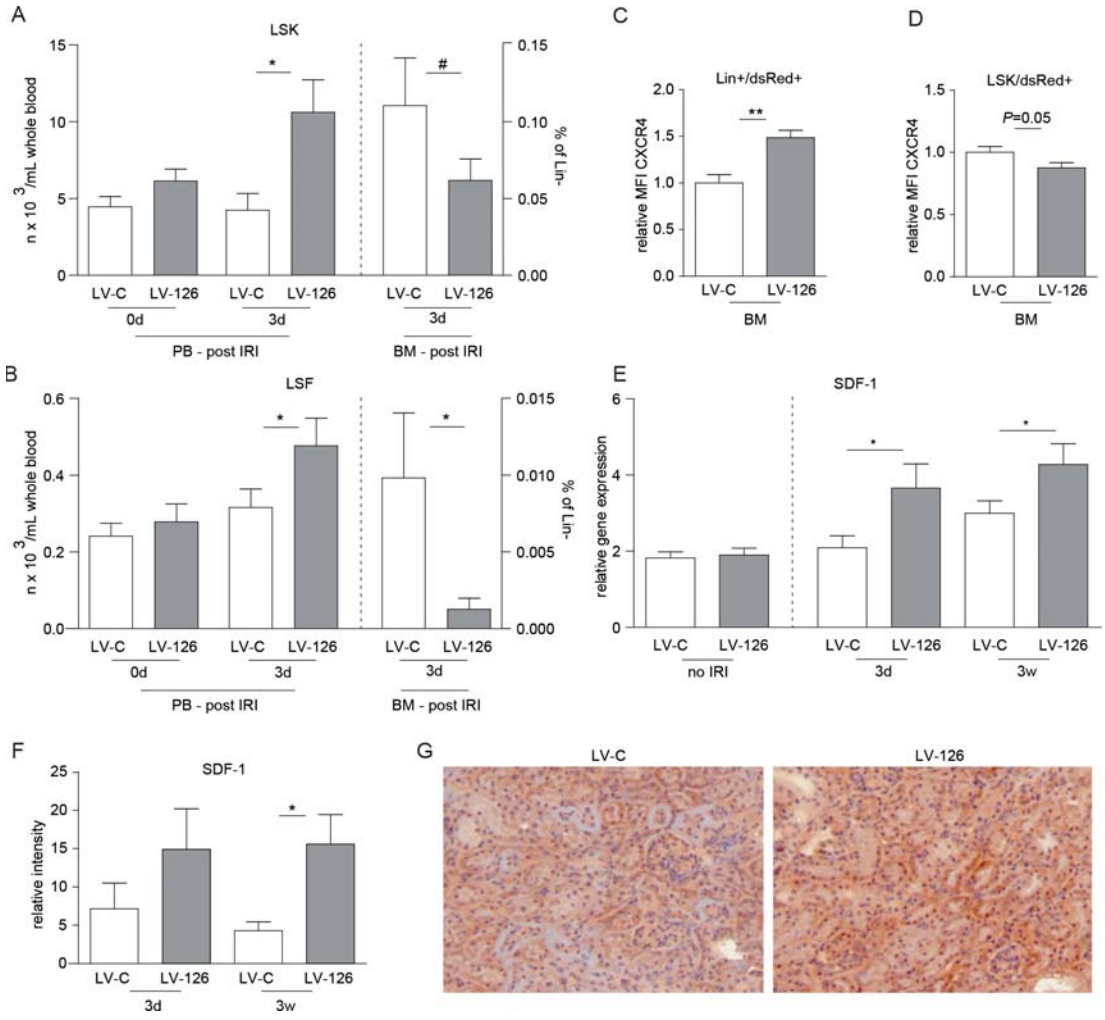

Figure 5. Overexpression of miR-126 results in increased hematopoietic stem/progenitor cell levels in PB and altered CXCR4/SDF-1 signaling. (A) FACS analysis of Lin-/Sca-1+/cKit+ (LSK) and (B) Lin-/Sca-1+/Flk+ (LSF) cells in PB and BM shows an increase of these circulating cells after injury after miR-126 overexpression. (C) FACS analysis on dsRed+/Lin+ cells shows an increased mean fluorescence intensity (MFI) for CXCR4 in LV-126 group, while (D) the dsRed+ LSK cells shows a decreased MFI for CXCR4 in LV-126 group. (E) qRT-PCR in kidneys shows increased SDF-1 mRNA levels in response to miR-126 overexpression in BM, while in non-ischemic kidneys this increase is absent. (F) Quantification and (G) representative microscopic images (3 days post IRI) of SDF-1 staining in kidney sections show increased SDF-1 expression in miR-126 overexpressing mice.

Table 1. Statistical analysis between different research indices. p=propability values; r= Spearman correlation coefficient. Values in bold are considered statistically significant ($p<0.05$).

	correlation	miR-126	LSK	LSF	urea	MECA	Kim-1	Kim-1	NGAL	dsRed
material		BM	PB	PB	serum	kidney	kidney	kidney	kidney	kidney
method		PCR	FACS	FACS		IHC	PCR	IHC	IHC	IHC
miR-126	p		**0.007**	0.34	0.46	0.53	0.65	0.15	0.36	**0.02**
	r		**0.65**	0.26	-0.20	0.20	-0.12	-0.38	-0.24	**0.58**
LSK PB	p	**0.007**		**0.004**	**0.020**	**0.008**	**0.03**	**0.04**	**0.04**	**0.03**
	r	**0.65**		**0.64**	**-0.54**	**0.68**	**-0.52**	**-0.50**	**-0.50**	**0.51**
LSF PB	p	0.34	**0.004**		**0.003**	**0.001**	**0.0005**	**0.03**	**0.001**	0.76
	r	0.26	**0.64**		**-0.66**	**0.77**	**-0.74**	**-0.51**	**-0.73**	0.08
MECA	p	0.53	**0.008**	**0.001**	**0.009**		**0.002**	**0.02**	**0.001**	0.96
	r	0.20	**0.68**	**0.77**	**-0.67**		**-0.75**	**-0.61**	**-0.77**	-0.02

(Figure 5C-D). This relative loss of CXCR4 expression on LSK cells in miR-126 overexpressing BM (Figure 5D) may cause the selective mobilization of these cells to the periphery (Figure 5A). On the other hand, recruitment of hematopoietic stem and progenitor cells to ischemic tissue is dependent on SDF-1 expression at the site of injury.[27, 39] As shown in Figure 5, in the tubuli of post-ischemic kidneys of LV-126 mice, both SDF-1 mRNA (5E) and protein expression (5F-G) were increased as compared to the LV-C mice both 3 days as well as 3 weeks after IRI, while SDF-1 mRNA expression levels were not changed in non-ischemic kidneys.

Discussion

Here we describe that overexpression of miR-126 in the hematopoietic compartment augments neovascularization in subcutaneously implanted matrigel plugs and protects the kidney from IRI. Protection of the kidney and vascular integrity correlated significantly with the levels of circulating vascular progenitor cells. In its turn, mobilization of LSK cells and the integration of dsRed^{+} cells in the renal microvascular network in the LV-126 mice were directly related to BM miR-126 expression levels. Therefore, our data support a direct causal role for miR-126 augmented vasculogenesis leading to the preservation of renal function following IRI.

One mechanism by which miR-126 augments vasculogenesis is by selectively enhancing the mobilization of potentially vasculogenic stem and progenitor cells. Elevated SDF-1 expression by the kidney following IRI is known to be a main driver of the homing of BM-derived progenitor cells to the injured kidney by altering the balance of SDF-1 expression from the BM to the periphery.[27, 39, 40] However, it has been demonstrated that plasma elevation of SDF-1 also mobilizes Lin^{+} leukocytes.[41] In our study, detailed flow cytometric analyses of the circulating hematopoietic cells in the LV-126 mice demonstrated selective mobilization of LSK and LSF cells in response to elevated SDF-1 expression by the ischemic kidney. A possible explanation for this observation could be that, in the BM, only the LSK cells displayed lower CXCR4 expression while the lineage-positive leukocytes expressed increased levels of CXCR4 and therefore would have a higher propensity to be retained in the BM.[38]

Several studies have described a regulatory role for miR-126 in SDF-1/CXCR4 signaling. MiR-126 was shown to target SDF-1 directly[33, 42] but also indirectly via targeting regulator of G protein signaling 16 (RGS16), a negative regulator of CXCR4 function. Silencing of RGS16 is thought to stimulate an autoregulatory feedback loop that increases the production of SDF-1.[43] Silencing of RGS16 by miR-126 could provide a mechanism for the elevated renal epithelial SDF-1 expression by the LV-126 mice. Although speculative, miR-126 could be increased in the tubular epithelial cells by lateral transfer through the fusion of miR-126 rich, blood cell derived microvesicles as it was recently described that injection of endothelial progenitior cell (EPC)-derived miR-126 rich microparticles exerted a protective effect in IRI.[44] Alternatively, the increased number of BM-derived EC that line the microvascular network of the kidney of the LV-126 mice could serve as a source of miR-126 via the production of microparticles,[45] as it was recently shown that, under certain

conditions, such particles can cross the tubular basement membrane.[46] In addition, activated platelets may be involved as miR-126 is among the most abundant miRNAs in platelets[47, 48] and they could serve as transporter of miR-126 to the site of injury[49]. As EPCs can take up platelets and their molecular content[50], platelets could also add to EPC function through miR-126 transfer. Furthermore, platelets have been shown to constitute a rich source of local SDF-1 deposition themselves[51].

We propose that preservation of the capillary density in the LV-126 kidneys following IR is a major contributor to the protected kidney function in the LV-126 mice. As this maintenance of vascular integrity after IR is associated with an enhanced incorporation of BM-derived dsRed$^+$ endothelial cells and pericytes we propose that overexpression of miR-126 in the hematopoietic compartment improves microvascular repair as compensation for the loss of capillaries. In addition, BM-derived EC and/or perivascular cells that had already been incorporated into the kidneys prior to IRI, could be more resistant to injury due to miR-126 dependent enhancement of pro-survival AKT signaling[30, 31] and therefore add to the protection after IRI.

Next to the effects on their mobilization, hematopoietic overexpression of miR-126 could also have direct beneficial effects on the function of vasculogenic stem and progenitor cells via its actions on AKT signaling.[29-31, 52] For instance, it was recently shown in preeclampsia that miR-126 modulates the proangiogenic properties of EPC through targeting PI3KR2,[53] which also appears to be affected in our study (Supplementary Figure 2). Augmenting AKT signaling in vascular progenitor cells could be particularly relevant in kidney disease as most patients are characterized by a state of EPC dysfunction.[54, 55] In addition, kidney graft function and the use of immunosuppressants were shown to directly affect EPC number and survival.[56-58]
In addition to BM-derived EC, we observed dsRed$^+$ cells expressing the pericyte marker PDGFRβ in the matrigel plug. Furthermore, a subpopulation of dsRed$^+$ cells in the kidney were shown to be most likely pericytes. This suggests that also pericytes originated from BM. Support for this notion is emerging in literature, where the role of BM-derived pericytes is increasingly discussed.[59, 60]

Taken together, we demonstrate that enhancing the vasculogenic potential by overexpression of miR-126 in the hematopoietic compartment protects the kidney from IRI further confirming the critical role of EC integrity in the progression of kidney disease. Therefore, strategies aimed at improvement of the endogenous vasculogenic potential such as described in this study would not only enhance the mobilization of the vasculogenic progenitors to the injured kidney but may also correct EPC dysfunction in renal disease.

Materials and Methods

Mice

C57BL/6J wild type (WT; CD45.2$^+$) and B6.SJL-Ptprca Pepcb/BoyCrl (CD45.1$^+$) mice were obtained from Charles River (Maastricht, the Netherlands). All animal experimental protocols were approved by the animal welfare committee of the Leiden University Medical Center.

Lentiviral vectors

Stable expression of miR-126 in BM-derived Lin$^-$ cells was accomplished using the vesicular stomatitis virus (VSV) G protein-pseudotyped self-inactivating human immunodeficiency virus type 1 (HIV1)-based vector LV.hU6.miRNA-126.hPGK1.DsRed.T4. In the shuttle plasmid for generating this vector, the coding sequence of murine miRNA-126 is preceded by the human U6 gene promoter and followed by a reporter gene cassette consisting of the human phosphoglycerate kinase 1 (hPGK1) gene promoter and the coding sequence of a rapidly maturing variant of the red fluorescent protein of *Discosoma spec.* (Supplementary Figure 1A).[61] The shuttle plasmid encoding the control vector LV.hPGK1.DsRed.T4 has the same genetic makeup as LV.hU6.miRNA-126.hPGK1.DsRed.T4 except for the absence of the human U6 gene promoter and murine miRNA-126-coding sequence (Supplementary Figure 1A). LV particles were produced in 293T cells with the aid of the packaging plasmids psPAX2 (Addgene, Cambridge, MA, USA) and pLP/VSVG (Invitrogen, Breda, the Netherlands) essentially as previously described.[62] At 48 h after the start of the transfection, the culture fluid was collected and freed of cellular debris by centrifugation at room temperature for 10 min at 825×*g* followed by filtration through a 0.45-μm pore-sized cellulose acetate filter (Pall, Port Washington, NY, USA). To concentrate the LV particles, 5 ml of 20% (wt/vol) sucrose (Merck, Whitehouse Station, NJ, USA) in phosphate-buffered saline (PBS) was carefully layered under 30 ml of the cleared culture medium, which was then centrifuged for 2 h at 15,000 rotations per minute for 2 h at 10ºC in an SW28 rotor (Beckman Coulter, Woerden, the Netherlands). Next, the supernatant was discarded and the pellet containing the LV particles was suspended in 500 μl of PBS-1% bovine serum albumin (BSA; Sigma-Aldrich, St. Louis, MO, USA) by gentle rocking overnight at 4ºC.

Transduction and transplantation of BM cells

BM cells were isolated from the femora and tibia of CD45.1$^+$ mice and were enriched for Lin$^-$ cells using a Lineage Cell Depletion Kit (Miltenyi

Biotec, Bergish Gladbach, Germany). Following isolation, Lin$^-$ cells (80-90% purity, Supplementary Figure 1B) were grown in StemSpan-SFEM (Stemcell Technologies Inc, Vancouver, BC, Canada) supplemented with 50 ng/mL recombinant mouse stem cell factor (rmSCF), 10 ng/mL recombinant mouse thrombopoietin (rmTPO) and 50 ng/mL recombinant mouse fms-related tyrosine kinase 3 ligand (rmFLT3-L) (all from R&D Systems, Minneapolis, MN, USA). After 24 h the cells were transduced with either LV.hU6. miRNA-126.hPGK1.DsRed.T4 or LV.hPGK1.DsRed.T4 by spin occulation in the presence of 4 μg/mL proteamine sulphate (Sigma Aldrich, St Louis, MO, USA) and maintained for another 24 h in supplemented StemSpan-SFEM. Transduced CD45.1 donor cells (300.000/mouse) were combined with supportive spleen cells (500.000/mouse) and injected into the tail vein of lethally irradiated (8 Gy) male C57BL/6J, CD45.2 acceptor mice.

Matrigel plug assay

Seven weeks after transplantation, mice were injected subcutaneously into the flank with 0.5 mL ice-cold matrigel (BD Biosciences, Breda, the Netherlands) supplemented with 100 ng/mL recombinant mouse SDF-1 (Invitrogen) and 50 ng/mL recombinant mouse VEGF (Invitrogen). After 7 days, the skin was opened to monitor the vasculature of the implants with a Sidestream Dark Field (SDF)-camera. Subsequently, implants were extracted, imaged with a Leica DMI6000microscope (Leica Microsystems, Rijswijk, the Netherlands) fixed in 4% paraformaldehyde and snap frozen at -80ºC. From all microscopic images of the matrigel implants the number of visual vessels were counted on both sides of the implants. To obtain the total length of the vessels, pictures were digitalized and the total pixel area of the vessels was calculated using ImageJ software (National Institutes of Health, Bethesda, Maryland, USA).

Mouse model for ischemia reperfusion injury

Eight weeks after transplantation the renal artery and vein of mice were clamped bilaterally for 15 minutes using surgical clamps (S&T, Neuhausen, Switzerland) followed by reperfusion as described previously.[63] Kidney function was determined by measuring urea in serum samples using standard auto-analyzer methods by our hospital research services. Kidneys were recovered either 72 hours or 3 weeks after reperfusion for immunohistological analyses and assessment of gene expression.

Immunohistology

Sections (4 μm) of snap-frozen kidneys were air-dried and acetone-fixed. Twenty μm sections of matrigel plugs were fixed with methanol on a glass

slide and subsequently blocked with 2% fetal calf serum (FCS, Bio Whittaker/ Cambrex, Verviers, Belgium), 3% bovine serum albumin (BSA, Sigma Aldrich) in PBS. For stainings involving horseradish peroxidase (HRP)-conjugated secondary antibodies, endogenous peroxidase was blocked with H_2O_2. Sections were then incubated with specific antibodies directed against murine KIM-1 (R&D systems), F4/80 (Abcam, Cambridge, UK), CD45 (Abcam), Gr-1 (a kind gift of G. Kraal, Vrije Universiteit Medisch Centrum, Amsterdam, the Netherlands), dsRed (LSBio, Seattle, WA, USA), MECA32 (Becton Dickinson, Franklin Lakes, New Jersey, USA), CD31 (FITC, Becton Dickinson), NG2 (Millipore), PDGFRβ (Abcam), SDF-1 (eBioscience, San Diego, CA, USA), vWF (Dako, Glostrup, Denmark), followed by appropriate secondary antibodies that were HRP-conjugated (Jackson Immunoresearch, Westgrove, PA, USA) or labeled with Alexa-488 or Alexa-568 (Molecular Probes). As negative control, isotype-matched IgGs were used. HRP-based stainings were visualized using Nova RED (Vector Labs, Peterborough, UK) and counterstained with hematoxylin. Mast cells were stained by toluidine blue (Sigma-Aldrich). Quantification of immunohistological staining results (expressed in pixels) was performed using image J software. Fluorescent micrographs were made using fluorescence microscopy (LSM 700, Zeiss, Germany) or confocal laser scanning microscopy (LSM 510, Zeiss). Quantification of $CD31^+dsRed^+$ double stained cells was performed in a blinded manner by manual counting. H&E staining was performed on snap-frozen kidney sections by standard methods. Histological evaluations for acute tubular necrosis and tubular cast formation were performed in a blinded manner by two independent observers.

RNA isolation and qRT-PCR analysis

Total RNA was isolated from kidney sections using Trizol reagent (Invitrogen). Reverse transcription was performed using a 5-minute 65ºC incubation of 250 ng total RNA with dNTPs (Invitrogen) and oligo(dT) (Invitrogen) or using specific Taqman® microRNA probes (miR-126, Applied Biosystems, Bleiswijk, the Netherlands). For mRNA detection, cDNA was synthesized using a M-MLV First-Strand Synthesis system (Invitrogen) and validation was carried out using SYBR Green Master Mix (Applied Biosystems). Primer sequences can be found in Supplementary Table 3. Levels of expression were determined by normalizing to GAPDH. Validation of miR-levels was performed using Taqman® miR assays (Applied Biosystems). MiR-levels were normalized on RNU6B levels obtained from the same RNA. Results were normalized using Gene Expression Analysis for iCycler IQ® RT-PCR Detection System (Bio-Rad Laboratories, Veenendaal, the Netherlands).

Flow cytometry and blood and bone marrow analysis

Whole blood was collected by incision of the tail vein or heart puncture and analyzed using a semi-automatic hematology analyzer (Sysmex F-280; Sysmex Corporation, Etten-Leur, the Netherlands), microscope (LSM 700, Leica) and flow cytometry (FACS, LSR II, BD Biosciences). Hematological values obtained included white blood cell counts (WBC, $n*10^6$/mL), red blood cell counts (RBC, $n*10^9$/mL), platelets (Plt, $n*10^6$/mL), hematocrit (Hct, %/%) and haemoglobin (Hgb, mmol/L). For microscopic images a smear was made from PB or BM and images were made using a fluorescence microscope. For FACS analysis, we incubated 35 μL of whole blood or 10^6 BM cells for 30 minutes at 4ºC with directly conjugated antibodies against CD45.1-PE-Cy7 (BD), CD45.2-APC-Cy7 (BD), B220-APC-Cy7 (eBioscience), CD11b-APC (Biolegend, San Diego, CA, USA), Ly6G-PE (BD), CD115-PerCP-Cy5.5 (R&D Systems) and Ly6C-FITC (Bioconnect, Huissen, The Netherlands). A separate sample was prepared for incubation with Sca-1-FITC (BD), CD117-PerCP-Cy5.5 (BD) and a cocktail against lineage-positive cells (APC-conjugated, BD). Likewise, samples were prepared for these markers in combination with staining for CXCR4 (MBL international, Woburn, MA, USA). After labeling, cell suspensions were washed with PBS containing 1% BSA (Sigma-Aldrich) and 0.01% sodium azide. Erythrocytes were removed by addition of lysis buffer (0.155 M NH_4Cl, 0.01 M KHCO3, 0.1 mM EDTA) and finally, cells were fixed with 1% paraformaldehyde. In a separate tube the sample was incubated with an appropriate cocktail of isotype controls. Data were analyzed using FACS-Diva software (BD Biosciences). The gating strategy for peripheral blood subpopulations is described in detail in Supplementary Figure 6.

Statistical Analysis

Results are expressed as mean ± standard error of the mean (SEM) unless stated otherwise. Statistical analysis was performed using students t-test. For correlation analysis Spearman's rank correlation coefficient was used. $P<0.05$ was considered statistically significant. Asterisks and hashtags were used to indicate levels of significance as follows: *; $P<0.05$, **; $P>0.01$, ***; $P<0.001$ and #; $P<0.10$.

Acknowledgements

We would like to thank Martijn H. Brugman and Kim J.M. Janssen for technical support. This work was supported by grants from the Dutch Heart Foundation (NHS 2006B145), Dutch Kidney Foundation (C07.2227 and C09.2329), Genzyme Renal Innovations Program and the Netherlands Institute of Regenerative Medicine.

Supplementary Files

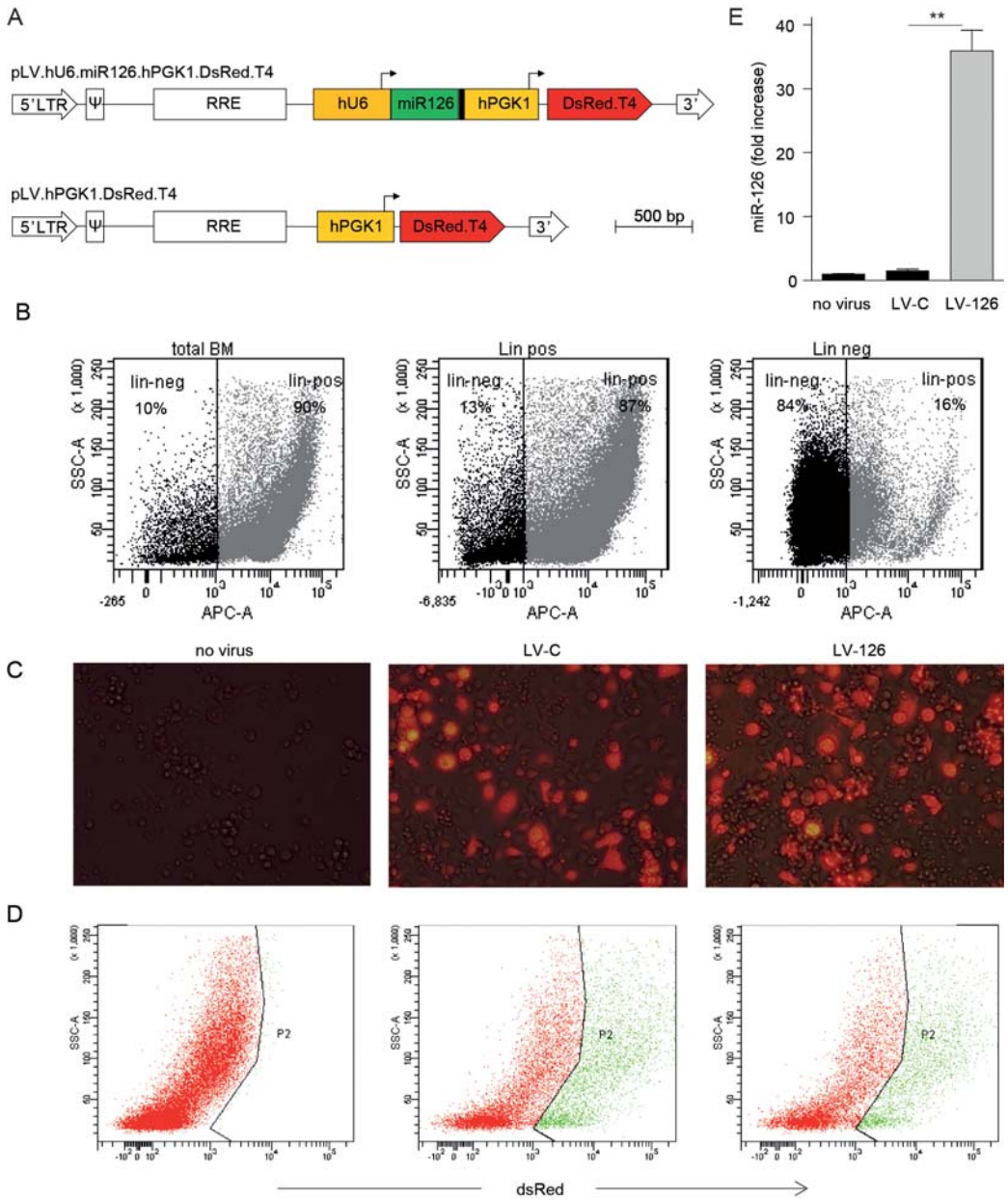

Supplementary Figure 1.

Supplementary Figure 1. Overexpression of miR-126 in Lin- bone marrow cells in vitro. (A) Schematic representation of the lentiviral miR-126 expression vector (pLV.hU6.miR126.hPGK1.DsRed.T4) (LV-126, upper scheme) and its control (pLV.hPGK1.DsRed.T4) (LV-C, lower scheme). A 445 bp PCR fragment (forward primer (Sal1): 5'-AAAAAAGTCGACGCGGAAGGCGGTGGGGACTCCC-3', reverse primer (BstB1): 5'-AAAAAATTCGAA CCAGAAGACTCAGGCCCAGGC-3') containing the precursor RNA hairpin for miR-126 flanked on both side by 180 nucleotides, was cloned downstream of the constitutive U6 promoter into the Sal1 and BstB1 cloning sites of vector pLV.hU6.hPGK1.DsRed.T4. Both vectors contain the dsRED reporter gene behind a PGK promoter to allow tracing of transduced cells. 5' LTR, chimeric 5' long terminal repeat containing the U3 region of Rous sarcoma virus coupled to the R and U5 regions of human immunodeficiency virus type 1 (HIV1); Ψ, HIV1 packaging signal; RRE, HIV1 Rev-responsive element; cPPT, HIV1 central polypurine tract and termination site; hU6, human U6 gene promoter; miR126, coding sequence of mouse miR-126; black box, RNA polymerase III transcriptional terminator, hPGK1, human phosphoglycerate kinase 1 gene promoter; DsRed.T4, coding sequence of a rapidly maturing variant of the Discosoma spec. red fluorescent protein61; 3' LTR, 3' HIV1 long terminal repeat containing a deletion in the U3 region to render the LV self-inactivating. (B) FACS plots showing APC-labeled Lin+ BM cells, before (left panel) and after negative selection for Lin+- cells (middle panel) and Lin- cells. (C) Fluorescent microscopy of Lin- cells, 2 days after transduction, shows a high number of fluorescent dsRed+ cells validating efficient transduction of the cells by both LC-V and LV-126. Non-transduced cells (no virus) are shown in the left panel as control. (D) FACS analysis of cells 5 days post transduction display an efficiency of about 30% for both constructs (P2 gate=green). (E) Quantitative rtPCR analysis (qPCR) five days after transduction showed a ~20-fold increase (n=3, $P<0.005$) in miR-126 expression levels in cells transduced with the LV-126 construct as compared to the LV-C construct and non-transduced BM cells (no virus).

A

Cell type/tissue	Target protein	Process	References
Endothelium, Hematopoietic stem cells, breast cancer	PI3KR2	vascular development, angiogenesis	1-3
Endothelium	RGS16	atherosclerosis, Sca1^{+} incorporation	4
CD4^{+} T cells	Dnmt1	DNA methylation	5
Hematopoietic stem cells	Hoxa9, c-Myb,	hematopoietic development, erythropoiesis	6, 7
Breast cancer	IGFBP2, PITPNC1	Suppression of metastatic angiogenesis	8
Breast and lung cancer	VEGF-A	Tumor growth	3, 9
Endothelium and mast cells	Spred-1	vascular development, angiogenesis, endothelial progenitor cell outgrowth	1, 10, 11

B

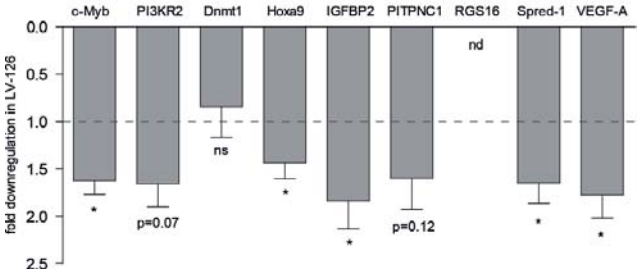

Supplementary Figure 2. Down regulation of established miR-126 targets. (A) overview of the selected miR-126 targets including details on proposed functions and relevant tissues. (B) qRT-PCR for established miR-126 targets in bone marrow (BM) shows downregulation in LV-126 mice as compared to LV-C mice. Of note,1-fold means no difference, ns = not significant and RGS16 gene expression was not detectable (nd).

1. Fish JE, Santoro MM, Morton SU, Yu S, Yeh RF, Wythe JD, Ivey KN, Bruneau BG, Stainier DY, Srivastava D. miR-126 regulates angiogenic signaling and vascular integrity. DevCell 15: 272-284, 2008.
2. Huang F, Fang ZF, Hu XQ, Tang L, Zhou SH, Huang JP. Overexpression of miR-126 promotes the differentiation of mesenchymal stem cells toward endothelial cells via activation of PI3K/Akt and MAPK/ERK pathways and release of paracrine factors. Biol Chem 394: 1223-1233, 2013.
3. Zhu N, Zhang D, Xie H, Zhou Z, Chen H, Hu T, Bai Y, Shen Y, Yuan W, Jing Q, Qin Y. Endothelial-specific intron-derived miR-126 is down-regulated in human breast cancer and targets both VEGFA and PIK3R2. MolCell Biochem 351: 157-164, 2011.
4. Zernecke A, Bidzhekov K, Noels H, Shagdarsuren E, Gan L, Denecke B, Hristov M, Koppel T, Jahantigh MN, Lutgens E, Wang S, Olson EN, Schober A, Weber C. Delivery of microRNA-126 by apoptotic bodies induces CXCL12-dependent vascular protection. SciSignal 2: ra81, 2009.
5. Zhao S, Wang Y, Liang Y, Zhao M, Long H, Ding S, Yin H, Lu Q. MicroRNA-126 regulates DNA methylation in CD4+ T cells and contributes to systemic lupus erythematosus by targeting DNA methyltransferase 1. Arthritis Rheum 63: 1376-1386, 2011.
6. Shen WF, Hu YL, Uttarwar L, Passegue E, Largman C. MicroRNA-126 regulates HOXA9 by binding to the homeobox. MolCell Biol 28: 4609-4619, 2008.
7. Grabher C, Payne EM, Johnston AB, Bolli N, Lechman E, Dick JE, Kanki JP, Look AT. Zebrafish microRNA-126 determines hematopoietic cell fate through c-Myb. Leukemia 25: 506-514, 2011.
8. Png KJ, Halberg N, Yoshida M, Tavazoie SF. A microRNA regulon that mediates endothelial recruitment and metastasis by cancer cells. Nature 481: 190-194, 2012.
9. Liu B, Peng XC, Zheng XL, Wang J, Qin YW. MiR-126 restoration down-regulate VEGF and inhibit the growth of lung cancer cell lines in vitro and in vivo. Lung Cancer 66: 169-175, 2009.
10. Wang S, Aurora AB, Johnson BA, Qi X, McAnally J, Hill JA, Richardson JA, Bassel-Duby R, Olson EN. The endothelial-specific microRNA miR-126 governs vascular integrity and angiogenesis. Dev Cell 15: 261-271, 2008.
11. Meng S, Cao JT, Zhang B, Zhou Q, Shen CX, Wang CQ. Downregulation of microRNA-126 in endothelial progenitor cells from diabetes patients, impairs their functional properties, via target gene Spred-1. J Mol Cell Cardiol 53: 64-72, 2012.

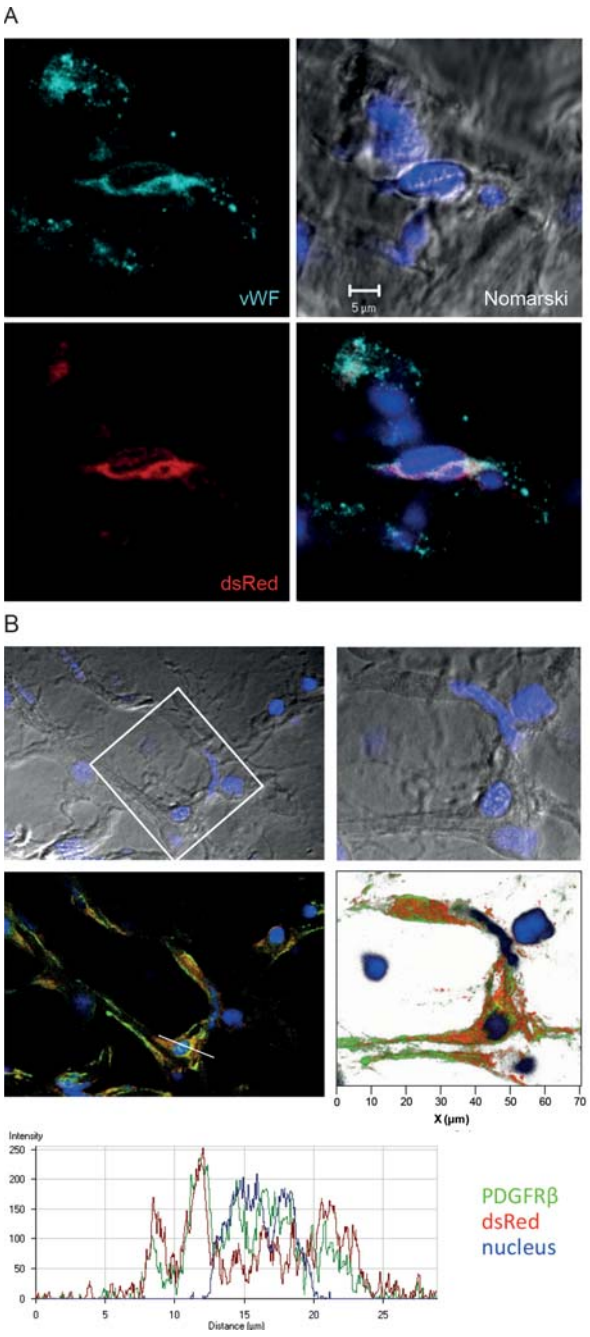

Supplementary Figure 3. DsRed+ endothelial cells and pericytes in vascular structures in matrigel. (A) Representative confocal images of a vessel stained for EC (vWF, green) and dsRed (red). (B) Representative confocal images of a zoomed region and corresponding cross sectional profiles of fluorescent labels (colors correspond to images) stained for PDGFRβ+/dsRed+ pericytes in LV-126 mouse. Right panels show zoom of region indicated by white square.

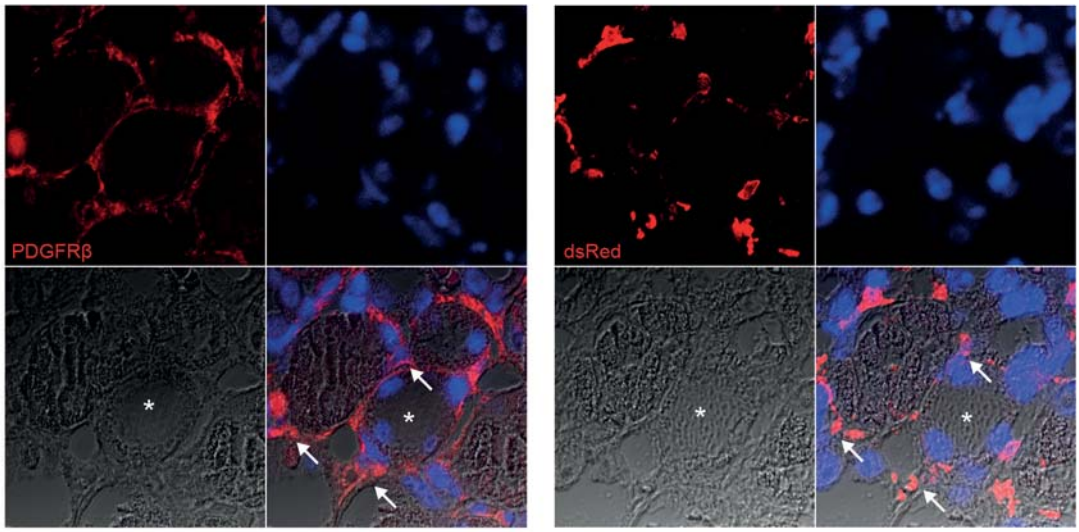

Supplementary Figure 4. Representative confocal images of sequential kidney sections of LV-126 mice showing structures positive for both PDGFRβ and dsRed (arrows). * represents corresponding tubuli.

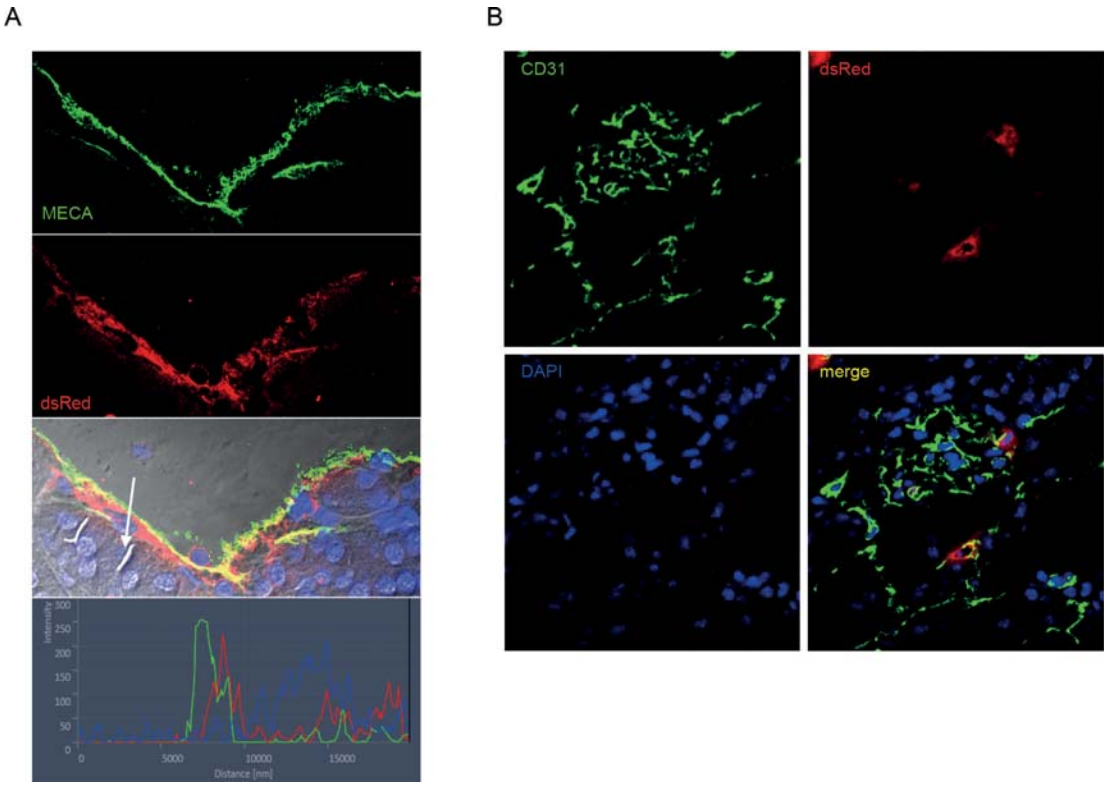

Supplementary Figure 5. DsRed-positive ECs in a large vessel and in a glomerulus. (A) representative confocal images of dsRed-positive ECs lining a large blood vessel and a cross sectional profile of fluorescent labels (colors correspond to images) shows overlap of MECA32 and dsRed. (B) Representative confocal images show a dsRed-positive glomerular CD31+ EC.

Supplementary Table 1. Hematological indices (Sysmex) and FACS analysis of whole blood. Values are expressed as mean numbers ± standard deviation of CD45.1 positive (donor derived) cells. Values in bold are significantly different (* $p<0.05$) between the LV-control and LV-126 group.

PB		Pre BMT	Post BMT & pre IRI				Post IRI			
		baseline	4w	4w	8w	8w	3d	3d	3w	3w
Sysmex	unit		LV-C	LV-126	LV-C	LV-126	LV-C	LV-126	LV-C	LV-126
WBC	n x 10^9/L	10.5 ± 1.3	7.4 ± 3.7	7.6 ± 3.0	14.2 ± 3.4	15.3 ± 4.3	8.5 ± 1.6	9.3 ± 2.5	12.5 ± 4.1	14.6 ± 3.2
RBC	n x 10^{12}/L	9.9 ±1.1	9.5 ±0.6	9.8 ±0.5	9.8 ±0.8	10.0 ±0.8	6.9 ±1.5	7.4 ±1.3	6.7 ±1.3	7.7 ±2.9
Plt	n x 10^9/L	972 ± 255	420 ± 192	504 ± 185	682 ± 158	714 ± 237	660 ± 287	712 ± 440	328 ± 266	391 ± 286
Hgb	mmol/L	9.6 ± 0.8	9.0 ± 0.5	9.2 ± 0.5	9.5 ± 0.6	9.5 ± 0.5	6.6 ± 1.4	7.0 ± 1.1	7.5 ± 1.5	8.4 ± 1.2
Hct	L/L	0.50 ± 0.04	0.49 ± 0.04	0.50 ± 0.02	0.51 ± 0.04	0.51 ± 0.04	0.34 ± 0.07	0.36 ± 0.07	0.31 ± 0.06	0.36 ± 0.14
FACS										
CD45.1+ WBCs	n x 10^6/mL	0.3 ± 0.1	6.1 ± 3.4	5.9 ± 2.5	11.4 ± 4.7	13.3 ± 4.2	7.6 ± 1.4	7.7 ± 2.3	10.5 ± 3.5	12.6 ± 3.2
T-cells	n x 10^6/mL	0.01 ± 0.02	0.29 ± 0.15	0.32 ± 0.28	1.19 ± 0.46	1.38 ± 0.59	1.07 ± 0.29	1.09 ± 0.22	1.08 ± 0.35	1.40 ± 0.22
B-cells	n x 10^6/mL	0.2 ± 0.0	2.5 ± 1.5	1.9 ± 1.1	5.8 ± 2.7	6.7 ± 2.6	2.8 ± 0.9	3.3 ± 1.2	4.5 ± 1.8	5.3 ± 1.7
NK-cells	n x 10^6/mL	0.00 ± 0.00	0.12 ± 0.06	0.14 ± 0.09	0.24 ± 0.13	0.22 ± 0.09	0.11 ± 0.05	0.10 ± 0.05	0.24 ± 0.13	0.30 ± 0.16
pDC	n x 10^6/mL	0.03 ± 0.02	**0.05 ± 0.03***	**0.03 ± 0.02***	0.12 ± 0.05	0.15 ± 0.07	0.05 ± 0.02	0.05 ± 0.02	**0.10 ± 0.03***	**0.16 ± 0.06***
Neutrophils	n x 10^6/mL	0.0 ± 0.0	2.1 ± 1.7	2.4 ± 1.7	1.8 ± 0.8	2.3 ± 1.4	2.2 ± 0.6	1.7 ± 0.9	2.5 ± 0.9	3.1 ± 1.7
Eosinophils	n x 10^6/mL	0.02 ± 0.01	0.25 ± 0.20	0.26 ± 0.30	0.42 ± 0.21	0.50 ± 0.23	0.59 ± 0.23	0.489 ± 0.32	0.38 ± 0.21	0.37 ± 0.19
Monocytes	n x 10^6/mL	0.04 ± 0.02	0.53 ± 0.35	0.69 ± 0.36	0.86 ± 0.37	0.93 ± 0.38	0.27 ± 0.16	0.28 ± 0.14	0.78 ± 0.26	0.81 ± 0.38
- Ly6C^{hi}		0.03 ± 0.02	0.33 ± 0.24	0.47 ± 0.30	0.42 ± 0.22	0.47 ± 0.20	0.09 ± 0.11	0.08 ± 0.07	0.45 ± 0.14	0.49 ± 0.26
- Ly6C^{med}		0.00 ± 0.00	0.07 ± 0.05	0.08 ± 0.04	0.10 ± 0.05	0.12 ± 0.06	0.01 ± 0.01	0.02 ± 0.01	0.10 ± 0.03	0.11 ± 0.07
- Ly6C^{lo}		0.01 ± 0.00	0.13 ± 0.08	0.14 ± 0.08	0.34 ± 0.14	0.33 ± 0.15	0.17 ± 0.07	0.18 ± 0.07	0.23 ± 0.11	0.19 ± 0.08

Supplementary Table 2. FACS analysis of bone marrow. Values are expressed as mean percentages ± standard deviation of CD45.1-positive (donor derived) cells. Values in bold are significantly different (* $p<0.05$. *** $p<0.001$) between the LV-control and LV-126 group.

BM		LV-C	LV-126	LV-C	LV-126
		3d post IRI	3d post IRI	3w post IRI	3w post IRI
CD45.1+ WBCs	(n x 10^6/mL)	81.6 ± 6.9	73.0 ± 15.2	82.6 ± 5.0	84.9 ± 5.5
T-cells	(n x 10^6/mL)	2.7 ± 0.5	2.7 ± 1.2	2.0 ± 0.8	1.6 ± 0.6
B-cells	(n x 10^6/mL)	8.5 ± 2.9	7.3 ± 2.6	6.2 ± 2.4	5.3 ± 1.7
NK-cells	(n x 10^6/mL)	2.5 ± 1.0	2.2 ± 1.1	**3.0 ± 0.5***	**2.0 ± 1.2***
pDC	(n x 10^6/mL)	**1.4 ± 0.6***	**0.8 ± 0.2***	0.7 ± 0.3	0.6 ± 0.1
Neutrophils	(n x 10^6/mL)	33.9 ± 5.3	30.7 ± 5.8	**45.8 ± 9.6***	**55.5 ± 4.6***
Eosinophils	(n x 10^6/mL)	4.9 ± 1.4	4.8 ± 3.2	1.9 ± 0.8	1.2 ± 0.7
Monocytes (all)	(n x 10^6/mL)	**23.6 ± 2.2***	**20.4 ± 2.6***	18.3 ± 2.6	12.7 ± 7.1
- Ly6C^{hi}		2.8 ± 1.8	3.0 ± 2.1	0.6 ± 0.4	0.4 ± 0.3
- Ly6C^{med}		**20.6 ± 1.3*****	**15.0 ± 3.8*****	16.7 ± 2.4	11.4 ± 6.3
- Ly6C^{lo}		0.6 ± 0.3	0.6 ± 0.3	0.7 ± 0.4	0.5 ± 0.3

Supplementary Table 3. Primers for qRT-PCR analysis.

Target Gene	Forward primer	Reverse primer
α-SMA	CGTGGCTATTCCTTCGTGAC	GCGTTCGTAGCTCTTCTCC
Col1 α1	TGACTGGAAGAGCGGAGAGT	GTTCGGGCTGATGTACCAGT
CCL2	GCACCAGCCAACTCTCAC	CTTCTTGGGGTCAGCACAG
IL-10	AATAAGAGCAAGGCAGTGGAG	CCCTGGATCAGATTTAGAGAGC
TGF-β	GCAACATGTGGAACTCTACCAGAA	GACGTCAAAAGACAGCCACTCA
Col3 α1	TCCCCTGGAATCTGTGAATC	TGAGTCGAATTGGGGAGAAT
Kim-1	GGGCTTCTATGTTGGCATC	TGTCTTCAGCTCGGGAATG
NGAL	GTTTCACCCGCTTTGCCAAG	CCACACTCACCACCCATTC
IL-6	ACAAAGCCAGAGTCCTTCAG	TGGTCTTGGTCCTTAGCC
SDF-1	CGTGAGGCCAGGGAAGAGT	TGATGAGCATGGTGGGTTGA
GAPDH	ACTCCCACTCTTCCACCTTC	CACCACCCTGTTGCTGTAG
U6	CTCGCTTCGGCAGCACA	AACGCTTCACGAATTTGCGT
PI3KR2	GGATGCCTGGCTTCAACGA	CTGGGAGTATGTGGCCTGACT
c-Myb	GAGCACCCAACTGTTCTCG	CACCAGGGGCCTGTTCTTAG
DNMT1	AAGAATGGTGTTGTCTACCGAC	CATCCAGGTTGCTCCCCTTG
IGFBP2	CAGACGCTACGCTGCTATCC	CCCTCAGAGTGGTCGTCATCA
PITPNC1	CAACCCATCATGTGCTCCTAC	CCCGAACATCATCCATTGTCAT
Hoxa9	TGGCCGAACACCCCG	CACCAAACACCGCCGC
RGS16	CGAGTGGGCCAGTAAGCATAA	CGAAAGACTCTCTCCATCCCAG
VEGF-A	GTACCTCCACCATGCCAAGT	GCATTCACATCTGCTGTGCT
Spred-1	GATGAGCGAGGAGACGGCGAC	GTCTCTGAGTCTCTCTCCACGGA

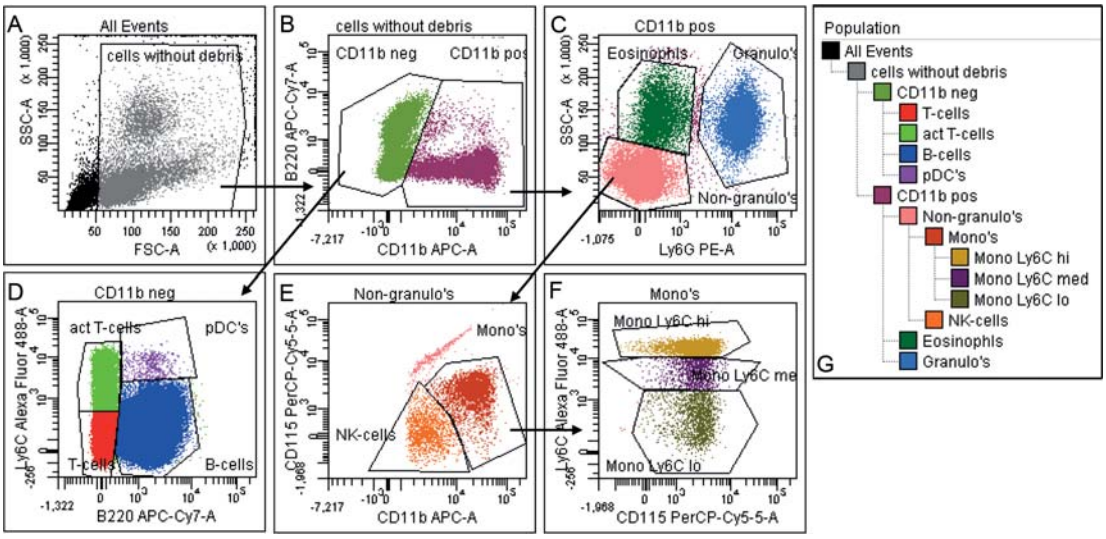

Supplementary Figure 6. Gating strategy for flow cytometry analysis. A gate is drawn on all cells in a FCS/SSC plot (A) to exclude debris. Of the cells gated in plot A, the expression of CD11b (X-axis) and B220 (Y-axis) is shown in plot B, on which gates are placed on the CD11b-neg cells and the CD11-pos cells. The CD11-pos cells are selected in plot C, showing expression of Ly6G (X-axis) and side scatter (SSC, Y-axis), in which Ly6G-pos/SSC-hi cells represent neutrophilic granulocytes, Ly6G-neg/ SSC-hi cells represent eosiniphilic granulocytes and the Ly6G-neg/SSC-lo cells represent the non-granulocytic cells. These latter cells are selected in plot E, showing their expression of CD11b (X-axis) and CD115 (Y-axis): CD11b-hi/CD115-hi cells represent the monocytes and the CD11b-dim/CD115-neg cells represent NK cells. The monocytes gated in plot E are selected in plot F, showing their expression of CD115 (X-axis) and Ly6C (Y-axis): Ly6C-hi cells represent the pro-inflammatory monocytes, Ly6C-med cells represent the intermediate monocyte population and Ly6C-lo cells represent the anti-inflammatory, pro-angiogenic/ repair-associated monocytes. The CD11b-neg cells gated in plot B are selected in plot D and show their expression of the B-cell marker B220 (X-axis) and Ly6C (Y-axis): B220-neg/Ly6C-neg cells represent the T-cells, B220-pos/Ly6C-neg cells are B-cells, B220-neg/Ly6C-pos cells are activated T-cells and B220-pos/Ly6C-pos cells are plasmacytoid dendritic cells (pDCs). All cells were analyzed within the CD45.1 group as these cells represent the donor cells.

References

1. Perico N, Cattaneo D, Sayegh MH, Remuzzi G. Delayed graft function in kidney transplantation. Lancet 364: 1814-1827, 2004.
2. Pagtalunan ME, Olson JL, Tilney NL, Meyer TW. Late consequences of acute ischemic injury to a solitary kidney. J Am Soc Nephrol 10: 366-373, 1999.
3. Sharfuddin AA, Molitoris BA. Pathophysiology of ischemic acute kidney injury. Nat Rev Nephrol 7: 189-200, 2011.
4. Bonventre JV, Yang L. Cellular pathophysiology of ischemic acute kidney injury. J Clin Invest 121: 4210-4221, 2011.
5. Flores J, DiBona DR, Beck CH, Leaf A. The role of cell swelling in ischemic renal damage and the protective effect of hypertonic solute. J Clin Invest 51: 118-126, 1972.
6. Lieberthal W, Wolf EF, Rennke HG, Valeri CR, Levinsky NG. Renal ischemia and reperfusion impair endothelium-dependent vascular relaxation. Am J Physiol 256: F894-900, 1989.
7. Kelly KJ, Williams WW, Jr., Colvin RB, Bonventre JV. Antibody to intercellular adhesion molecule 1 protects the kidney against ischemic injury. Proc Natl Acad Sci U S A 91: 812-816, 1994.
8. Basile DP, Donohoe D, Roethe K, Osborn JL. Renal ischemic injury results in permanent damage to peritubular capillaries and influences long-term function. Am J Physiol Renal Physiol 281: F887-899, 2001.
9. Fligny C, Duffield JS. Activation of pericytes: recent insights into kidney fibrosis and microvascular rarefaction. Curr Opin Rheumatol 25: 78-86, 2013.
10. Spurgeon KR, Donohoe DL, Basile DP. Transforming growth factor-beta in acute renal failure: receptor expression, effects on proliferation, cellularity, and vascularization after recovery from injury. Am J Physiol Renal Physiol 288: F568-577, 2005.
11. Ishii Y, Sawada T, Kubota K, Fuchinoue S, Teraoka S, Shimizu A. Injury and progressive loss of peritubular capillaries in the development of chronic allograft nephropathy. Kidney Int 67: 321-332, 2005.
12. Namikoshi T, Satoh M, Horike H, Fujimoto S, Arakawa S, Sasaki T, Kashihara N. Implication of peritubular capillary loss and altered expression of vascular endothelial growth factor in IgA nephropathy. Nephron Physiol 102: p9-16, 2006.
13. Basile DP, Friedrich JL, Spahic J, Knipe N, Mang H, Leonard EC, Changizi-Ashtiyani S, Bacallao RL, Molitoris BA, Sutton TA. Impaired endothelial proliferation and mesenchymal transition contribute to vascular rarefaction following acute kidney injury. Am J Physiol Renal Physiol 300: F721-733, 2011.
14. Rabelink TJ, de Boer HC, van Zonneveld AJ. Endothelial activation and circulating markers of endothelial activation in kidney disease. Nat Rev Nephrol 6: 404-414, 2010.
15. Jung YJ, Kim DH, Lee AS, Lee S, Kang KP, Lee SY, Jang KY, Sung MJ, Park SK, Kim W. Peritubular capillary preservation with COMP-angiopoietin-1 decreases ischemia-reperfusion-induced acute kidney injury. Am J Physiol Renal Physiol 297: F952-960, 2009.
16. Lin SL, Chang FC, Schrimpf C, Chen YT, Wu CF, Wu VC, Chiang WC, Kuhnert F, Kuo CJ, Chen YM, Wu KD, Tsai TJ, Duffield JS. Targeting endothelium-pericyte cross talk by inhibiting VEGF receptor signaling attenuates kidney microvascular rarefaction and fibrosis. Am J Pathol 178: 911-923, 2011.
17. Long DA, Price KL, Ioffe E, Gannon CM, Gnudi L, White KE, Yancopoulos GD, Rudge JS, Woolf AS. Angiopoietin-1 therapy enhances fibrosis and inflammation following folic acid-induced acute renal injury. Kidney Int 74: 300-309, 2008.

18. Schrimpf C, Xin C, Campanholle G, Gill SE, Stallcup W, Lin SL, Davis GE, Gharib SA, Humphreys BD, Duffield JS. Pericyte TIMP3 and ADAMTS1 modulate vascular stability after kidney injury. J Am Soc Nephrol 23: 868-883, 2012.
19. Long DA, Norman JT, Fine LG. Restoring the renal microvasculature to treat chronic kidney disease. Nat Rev Nephrol 8: 244-250, 2012.
20. Becherucci F, Mazzinghi B, Ronconi E, Peired A, Lazzeri E, Sagrinati C, Romagnani P, Lasagni L. The role of endothelial progenitor cells in acute kidney injury. Blood Purif 27: 261-270, 2009.
21. Rookmaaker MB, Smits AM, Tolboom H, Van 't Wout K, Martens AC, Goldschmeding R, Joles JA, Van Zonneveld AJ, Grone HJ, Rabelink TJ, Verhaar MC. Bone-marrow-derived cells contribute to glomerular endothelial repair in experimental glomerulonephritis. Am J Pathol 163: 553-562, 2003.
22. Li B, Cohen A, Hudson TE, Motlagh D, Amrani DL, Duffield JS. Mobilized human hematopoietic stem/progenitor cells promote kidney repair after ischemia/reperfusion injury. Circulation 121: 2211-2220, 2010.
23. Patschan D, Krupincza K, Patschan S, Zhang Z, Hamby C, Goligorsky MS. Dynamics of mobilization and homing of endothelial progenitor cells after acute renal ischemia: modulation by ischemic preconditioning. Am J Physiol Renal Physiol 291: F176-185, 2006.
24. Li J, Deane JA, Campanale NV, Bertram JF, Ricardo SD. The contribution of bone marrow-derived cells to the development of renal interstitial fibrosis. Stem Cells 25: 697-706, 2007.
25. Lagaaij EL, Cramer-Knijnenburg GF, van Kemenade FJ, van Es LA, Bruijn JA, van Krieken JH. Endothelial cell chimerism after renal transplantation and vascular rejection. Lancet 357: 33-37, 2001.
26. Asahara T, Murohara T, Sullivan A, Silver M, van der Zee R, Li T, Witzenbichler B, Schatteman G, Isner JM. Isolation of putative progenitor endothelial cells for angiogenesis. Science 275: 964-967, 1997.
27. Togel F, Isaac J, Hu Z, Weiss K, Westenfelder C. Renal SDF-1 signals mobilization and homing of CXCR4-positive cells to the kidney after ischemic injury. Kidney Int 67: 1772-1784, 2005.
28. Zheng H, Fu G, Dai T, Huang H. Migration of endothelial progenitor cells mediated by stromal cell-derived factor-1alpha/CXCR4 via PI3K/Akt/eNOS signal transduction pathway. J Cardiovasc Pharmacol 50: 274-280, 2007.
29. Asgeirsdottir SA, van Solingen C, Kurniati NF, Zwiers PJ, Heeringa P, van Meurs M, Satchell SC, Saleem MA, Mathieson PW, Banas B, Kamps JA, Rabelink TJ, van Zonneveld AJ, Molema G. MicroRNA-126 contributes to renal microvascular heterogeneity of VCAM-1 protein expression in acute inflammation. Am J Physiol Renal Physiol 302: F1630-1639, 2012.
30. Fish JE, Santoro MM, Morton SU, Yu S, Yeh RF, Wythe JD, Ivey KN, Bruneau BG, Stainier DY, Srivastava D. miR-126 regulates angiogenic signaling and vascular integrity. Dev Cell 15: 272-284, 2008.
31. Harris TA, Yamakuchi M, Ferlito M, Mendell JT, Lowenstein CJ. MicroRNA-126 regulates endothelial expression of vascular cell adhesion molecule 1. Proc Natl Acad Sci U S A 105: 1516-1521, 2008.
32. Salvucci O, Jiang K, Gasperini P, Maric D, Zhu J, Sakakibara S, Espigol-Frigole G, Wang S, Tosato G. MicroRNA126 contributes to granulocyte colony-stimulating factor-induced hematopoietic progenitor cell mobilization by reducing the expression of vascular cell adhesion molecule 1. Haematologica 97: 818-826, 2012.
33. van Solingen C, de Boer HC, Bijkerk R, Monge M, van Oeveren-Rietdijk AM, Seghers L, de Vries MR, van der Veer EP, Quax PH, Rabelink TJ, van Zonneveld AJ. MicroRNA-126 modulates endothelial SDF-1 expression and mobilization of Sca-1(+)/Lin(-) progenitor cells in ischaemia. Cardiovasc Res 92: 449-455, 2011.

34. Ishizaki T, Tamiya T, Taniguchi K, Morita R, Kato R, Okamoto F, Saeki K, Nomura M, Nojima Y, Yoshimura A. miR126 positively regulates mast cell proliferation and cytokine production through suppressing Spred1. Genes Cells 16: 803-814, 2011.

35. Kim J, Seok YM, Jung KJ, Park KM. Reactive oxygen species/oxidative stress contributes to progression of kidney fibrosis following transient ischemic injury in mice. Am J Physiol Renal Physiol 297: F461-470, 2009.

36. Yoder MC. Endothelial progenitor cell: a blood cell by many other names may serve similar functions. J Mol Med (Berl) 91: 285-295, 2013.

37. Loomans CJ, Wan H, de Crom R, van Haperen R, de Boer HC, Leenen PJ, Drexhage HA, Rabelink TJ, van Zonneveld AJ, Staal FJ. Angiogenic murine endothelial progenitor cells are derived from a myeloid bone marrow fraction and can be identified by endothelial NO synthase expression. Arterioscler Thromb Vasc Biol 26: 1760-1767, 2006.

38. Broxmeyer HE, Orschell CM, Clapp DW, Hangoc G, Cooper S, Plett PA, Liles WC, Li X, Graham-Evans B, Campbell TB, Calandra G, Bridger G, Dale DC, Srour EF. Rapid mobilization of murine and human hematopoietic stem and progenitor cells with AMD3100, a CXCR4 antagonist. J Exp Med 201: 1307-1318, 2005.

39. Ceradini DJ, Kulkarni AR, Callaghan MJ, Tepper OM, Bastidas N, Kleinman ME, Capla JM, Galiano RD, Levine JP, Gurtner GC. Progenitor cell trafficking is regulated by hypoxic gradients through HIF-1 induction of SDF-1. Nat Med 10: 858-864, 2004.

40. Hattori K, Heissig B, Rafii S. The regulation of hematopoietic stem cell and progenitor mobilization by chemokine SDF-1. Leuk Lymphoma 44: 575-582, 2003.

41. Hattori K, Heissig B, Tashiro K, Honjo T, Tateno M, Shieh JH, Hackett NR, Quitoriano MS, Crystal RG, Rafii S, Moore MA. Plasma elevation of stromal cell-derived factor-1 induces mobilization of mature and immature hematopoietic progenitor and stem cells. Blood 97: 3354-3360, 2001.

42. Zhang Y, Yang P, Sun T, Li D, Xu X, Rui Y, Li C, Chong M, Ibrahim T, Mercatali L, Amadori D, Lu X, Xie D, Li QJ, Wang XF. miR-126 and miR-126(*) repress recruitment of mesenchymal stem cells and inflammatory monocytes to inhibit breast cancer metastasis. Nat Cell Biol 15: 284-294, 2013.

43. Zernecke A, Bidzhekov K, Noels H, Shagdarsuren E, Gan L, Denecke B, Hristov M, Koppel T, Jahantigh MN, Lutgens E, Wang S, Olson EN, Schober A, Weber C. Delivery of microRNA-126 by apoptotic bodies induces CXCL12-dependent vascular protection. Sci Signal 2: ra81, 2009.

44. Cantaluppi V, Gatti S, Medica D, Figliolini F, Bruno S, Deregibus MC, Sordi A, Biancone L, Tetta C, Camussi G. Microvesicles derived from endothelial progenitor cells protect the kidney from ischemia-reperfusion injury by microRNA-dependent reprogramming of resident renal cells. Kidney Int 82: 412-427, 2012.

45. Zhou J, Li JY, Nguyen P, Wang KC, Weiss A, Kuo YC, Chiu JJ, Shyy JY, Chien S. Regulation of Vascular Smooth Muscle Cell Turnover by Endothelial Cell-secreted MicroRNA-126: Role of Shear Stress. Circ Res, 2013.

46. Borges FT, Melo SA, Ozdemir BC, Kato N, Revuelta I, Miller CA, Gattone VH, 2nd, LeBleu VS, Kalluri R. TGF-beta1-containing exosomes from injured epithelial cells activate fibroblasts to initiate tissue regenerative responses and fibrosis. J Am Soc Nephrol 24: 385-392, 2013.

47. de Boer HC, van Solingen C, Prins J, Duijs JM, Huisman MV, Rabelink TJ, van Zonneveld AJ. Aspirin treatment hampers the use of plasma microRNA-126 as a biomarker for the progression of vascular disease. Eur Heart J, 2013.

48. Nagalla S, Shaw C, Kong X, Kondkar AA, Edelstein LC, Ma L, Chen J, McKnight GS, Lopez JA, Yang L, Jin Y, Bray MS, Leal SM, Dong JF, Bray PF. Platelet microRNA-mRNA coexpression profiles correlate with platelet reactivity. Blood 117: 5189-5197, 2011.

49. Zampetaki A, Willeit P, Tilling L, Drozdov I, Prokopi M, Renard JM, Mayr A, Weger S, Schett G, Shah A, Boulanger CM, Willeit J, Chowienczyk PJ, Kiechl S, Mayr M. Prospective Study on Circulating MicroRNAs and Risk of Myocardial Infarction. J Am Coll Cardiol 60: 290-299, 2012.
50. Bitzer M, Ben-Dov IZ, Thum T. Microparticles and microRNAs of endothelial progenitor cells ameliorate acute kidney injury. Kidney Int 82: 375-377, 2012.
51. Massberg S, Konrad I, Schurzinger K, Lorenz M, Schneider S, Zohlnhoefer D, Hoppe K, Schiemann M, Kennerknecht E, Sauer S, Schulz C, Kerstan S, Rudelius M, Seidl S, Sorge F, Langer H, Peluso M, Goyal P, Vestweber D, Emambokus NR, Busch DH, Frampton J, Gawaz M. Platelets secrete stromal cell-derived factor 1alpha and recruit bone marrow-derived progenitor cells to arterial thrombi in vivo. J Exp Med 203: 1221-1233, 2006.
52. Dimmeler S, Aicher A, Vasa M, Mildner-Rihm C, Adler K, Tiemann M, Rutten H, Fichtlscherer S, Martin H, Zeiher AM. HMG-CoA reductase inhibitors (statins) increase endothelial progenitor cells via the PI 3-kinase/Akt pathway. J Clin Invest 108: 391-397, 2001.
53. Yan T, Liu Y, Cui K, Hu B, Wang F, Zou L. MiR-126 regulates EPCs function: implications for a role of miR-126 in preeclampsia. J Cell Biochem, 2013.
54. Goligorsky MS, Yasuda K, Ratliff B. Dysfunctional endothelial progenitor cells in chronic kidney disease. J Am Soc Nephrol 21: 911-919, 2010.
55. Reinders ME, Rabelink TJ, Briscoe DM. Angiogenesis and endothelial cell repair in renal disease and allograft rejection. J Am Soc Nephrol 17: 932-942, 2006.
56. Davies WR, Wang S, Oi K, Bailey KR, Tazelaar HD, Caplice NM, McGregor CG. Cyclosporine decreases vascular progenitor cell numbers after cardiac transplantation and attenuates progenitor cell growth in vitro. J Heart Lung Transplant 24: 1868-1877, 2005.
57. de Groot K, Bahlmann FH, Bahlmann E, Menne J, Haller H, Fliser D. Kidney graft function determines endothelial progenitor cell number in renal transplant recipients. Transplantation 79: 941-945, 2005.
58. Imanishi T, Kobayashi K, Kuki S, Takahashi C, Akasaka T. Sirolimus accelerates senescence of endothelial progenitor cells through telomerase inactivation. Atherosclerosis 189: 288-296, 2006.
59. Dar A, Domev H, Ben-Yosef O, Tzukerman M, Zeevi-Levin N, Novak A, Germanguz I, Amit M, Itskovitz-Eldor J. Multipotent vasculogenic pericytes from human pluripotent stem cells promote recovery of murine ischemic limb. Circulation 125: 87-99, 2012.
60. Tigges U, Hyer EG, Scharf J, Stallcup WB. FGF2-dependent neovascularization of subcutaneous Matrigel plugs is initiated by bone marrow-derived pericytes and macrophages. Development 135: 523-532, 2008.
61. Bevis BJ, Glick BS. Rapidly maturing variants of the Discosoma red fluorescent protein (DsRed). Nat Biotechnol 20: 83-87, 2002.
62. Ramkisoensing AA, Pijnappels DA, Swildens J, Goumans MJ, Fibbe WE, Schalij MJ, de Vries AA, Atsma DE. Gap junctional coupling with cardiomyocytes is necessary but not sufficient for cardiomyogenic differentiation of cocultured human mesenchymal stem cells. Stem Cells 30: 1236-1245, 2012.
63. de Vries DK, Lindeman JH, Tsikas D, de Heer E, Roos A, de Fijter JW, Baranski AG, van Pelt J, Schaapherder AF. Early renal ischemia-reperfusion injury in humans is dominated by IL-6 release from the allograft. Am J Transplant 9: 1574-1584, 2009.